



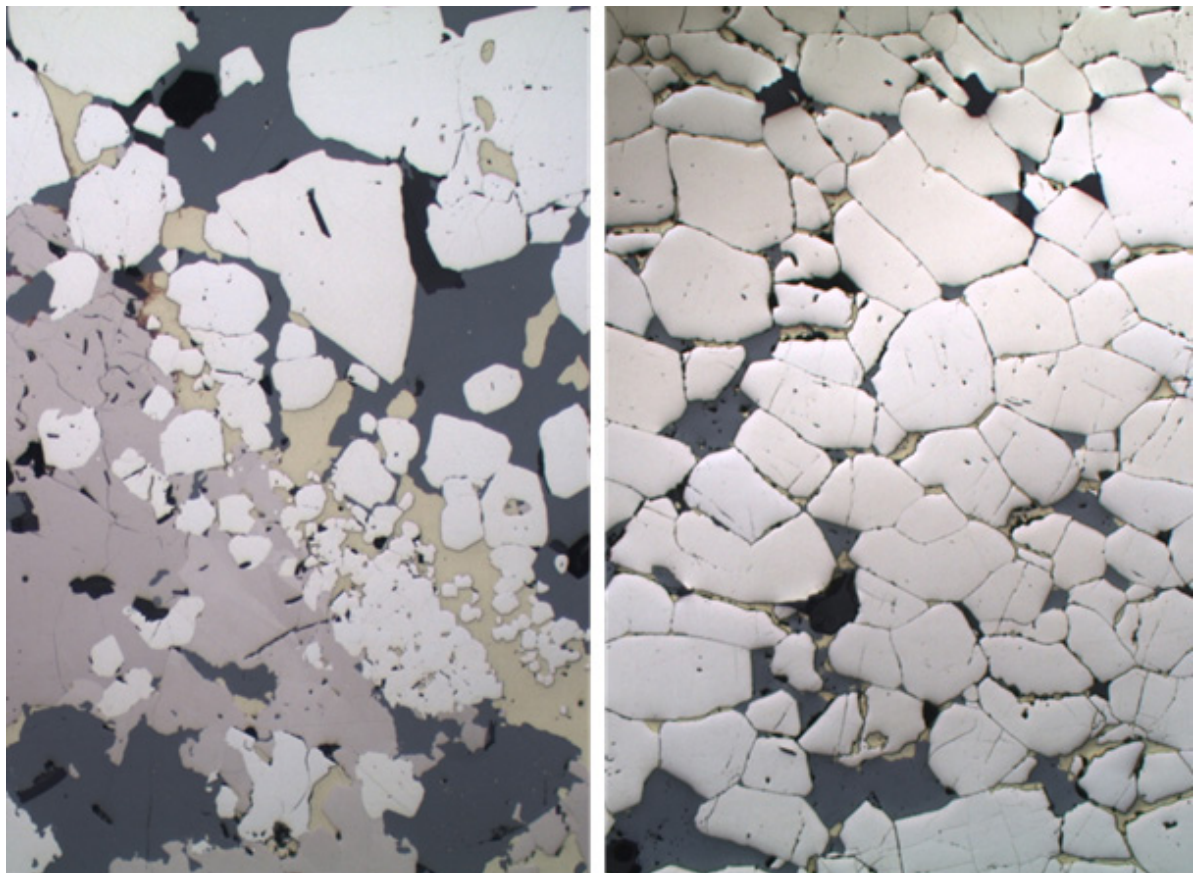
Stockholm
University

Bachelor Thesis

Degree Project in
Geology 15 hp

Sulphide mineralogy and the distribution of Au in the Westwood VMS deposit, Canada

Evelina Rann



Stockholm 2017

Department of Geological Sciences
Stockholm University
SE-106 91 Stockholm
Sweden

Abstract

The Westwood deposit is located within the Doyon-Bousquet-LaRonde mining camp in the Abitibi Greenstone belt in eastern Canada. It is a volcanic massive sulphide (VMS) deposit of late Archean age and is mined for its precious metals (Au and Ag) and contain also significant amount of base metals (Cu, Zn, Pb). It is important both in terms of our understanding of how the deposit formed, and also in terms of processing of the ore to understand where Au is located, and in what grade it could be extracted from a deposit for it to be profitable to be mined. Identifying the settings, mineralogy and the geological processes that favour precious metals are crucial for beneficial mining.

This study examines the mineralogy and mineral chemistry of eight samples collected from the Westwood deposit, with the focus on the sulphide grains. The main sulphide minerals are pyrite, sphalerite, chalcopyrite, pyrrhotite and galena. Six of the samples were further analysed with SEM and two of these (one Au-rich and one Au-poor) were also examined with LA-ICP-MS to investigate the quantity of Au within the samples. The interest of these examinations is not only to estimate the amount of Au within the sulphides but also to see if Au is favoured in a certain mineral with a specific lithology. The results show that Au is present in sulphide minerals in both samples analysed with LA-ICP-MS. The highest content in the Au-rich sample is within pyrrhotite, and in WE-7 there are high peaks in two analyses with sphalerite and pyrite. The main host for Au is electrum (an Au-Ag alloy) which only occurs in the Au-rich sample. The textures of pyrite indicate remobilisation of Au from the sulphides to form electrum in locations with less strain during metamorphism.

Table of contents

1. Introduction.....	4
1.1 Aim of the project.....	4
2. Background literature review.....	6
2.1 VMS deposits.....	6
2.2 Au concentration in VMS deposits.....	7
2.3 Geological setting.....	7
2.4 Au enrichment in Westwood deposit.....	10
3. Methods.....	11
3.1 The SEM	11
3.2 The LA-ICP-MS	11
4. Results and description of samples	13
4.1 Microscopy.....	13
4.2 SEM results	26
4.3 LA-ICP-MS results	29
5. Discussion.....	33
5.1 Comparison of samples	33
5.2 Interpretation of SEM and LA-ICP-MS data	33
5.3 Au enrichment in samples.....	35
5.4 Comparing Westwood deposit to Boliden Au-deposit.....	37
5.5 Significance of study	37
6. Conclusion	38
7. Acknowledgements	38
8. References	39

1. Introduction

Westwood Au-rich VMS deposit lies in the Abitibi Belt in eastern Canada. The Abitibi belt comprise of a greenbelt of late Archean age that has been subjected to deformation and metamorphism. The Westwood deposit occurs within Doyon-Bousquet-LaRonde (DBL) mining camp within Blake River Group (BRG) (Mercier-Langevin et al., 2009). DBL is a part of the BRG which hosts many of the VMS deposits in Canada. The Westwood deposit is one of the later discovered deposit in the area. The Au-rich sulphide zones and veins at the surface in Blake River group were discovered in the 1930's, and in 1938, a short period of mining resulted in 3 tons with 200 g/t Au. Production was then halted for an extended period, before it was resumed in 2013. It is mined for its high content of precious and base metals that are distributed within volcanic massive sulphides and sulphide rich veins (Yergeau et al., 2014).

The homoclinic sequence in BRG is dipping steeply to the south and during formation of this location, there were discharge of hot hydrothermal fluids, rich in metals, that have leached and formed massive sulphide lenses. Both the ore zones and the alteration zones are metamorphosed to upper greenschist and lower amphibolite facies. (Yergeau et al., 2014). The ore zones in Westwood are close to surface and extend to a depth of about 2.5 km. The ore zones consist of multiple layers where there are gold poor and gold rich lenses. The ore zones are located in three corridors in Westwood: Zone 2 Extension, North Corridor and Westwood Corridor (Yergeau et al., 2014). These lenses became elongated during a second deformation event which also had the largest impact of recrystallization of sulphide grains. The lenses in Westwood are disseminated massive sulphides and quartz-rich veins. The main sulphide mineralogy is pyrite, sphalerite, chalcopyrite, pyrrhotite and galena (Yergeau et al., 2014).

VMS deposits can contain both Au-rich and Au-poor ore zones, and this is the case for Westwood. They can occur adjacent to each other, but commonly show a difference in mineralogical abundance, where there is higher diversity in types of minerals in Au-rich zones (Dubé and Gosselin et al., 2007).

1.1 Aim of the project

The aim of this project was to constrain the mineralogy of a collection of samples, with focus on the sulphides, from the Westwood Au-rich volcanogenic massive sulphide (VMS) deposit in the Abitibi Belt, Canada. The deposit hosts over 40 different sulphide horizons, some of which are Au-rich, some of which are Au-poor or barren. The sample suite collected includes both Au-rich and Au-poor sulphide samples and the key focus was to investigate the mineralogical differences between these two samples with the aid of LA-ICP-MS. This was done to identify the mineral hosts for Au in the Au-rich sample. The samples investigated, listed with sample names and lithologies, are shown in **Table 1**.

Table 1. Samples investigated in this study with a description of the lithology.

Sample number	Lithology
WE-1	Least altered dacite
WE-2	Sericite altered basaltic andesite
WE-3	Sericite-pyrite altered dacite
WE-4	Stringer zone massive sulphide in dacite
WE-5	Massive sulphide – banded sphalerite-pyrite Au-rich
WE-6	Massive sulphide – banded sphalerite-pyrite ore with quartz lens. Au-rich
WE-7	Massive sulphide – pyrite-rich. Au-poor
WE-8	Least altered dacite above ore lens

2. Background literature review

2.1 VMS deposits

Volcanic massive sulphide (VMS) deposits are hydrothermal ore deposits that can form in volcanic or sedimentary host rocks. The oldest VMS deposits are 3.4 Ga, there are about 800 deposits all over the world, and many of the largest have formed during the Archean or Paleoproterozoic age (Galley et al., 2007). These deposits are also known to be actively forming on ocean spreading ridges in the present day. VMS deposits are commonly exploited for base metals (Pb, Zn, Cu) but a small group of deposits are also enriched in Au and Ag (Galley et al., 2007). The polymetallic nature makes them an attractive target for the exploration industry as the larger number of metals protects against fluctuation of metal prices (Galley et al., 2007).

VMS deposits form in or just below the seafloor in extensional settings such as mid-ocean ridges or extensional arc settings where hydrothermal fluids move upwards from deeper levels in the oceanic crust through synvolcanic faults. Crustal thinning of the lithosphere enables the mantle to rise and cause extension of the continental plates to preserve a high concentrated heat and form hydrothermal circulation that is needed for the formation of VMS deposits. The hydrothermal fluids are commonly considered to come from two main sources; either seawater that has infiltrated deep into the oceanic crust, leaching metals as it moves through the rock, and magmatic fluids exsolved from crystallising plutons at depth (Gibson et al., 2007). The hot metal-rich hydrothermal fluid becomes focused into the fault zones as it rises and deposits sulphide minerals due to temperature or redox changes as it vents from the oceanic crust into cold seawater, or as it infiltrates permeable sedimentary layers causing replacement type mineralisation (Gibson et al., 2007).

There are several classifications of VMS deposits depending on base metal-content, the Au content and their host rock. The base-metal compositions are classified by the ratio of Cu-Zn, Zn-Cu and Zn-Pb-Cu (Galley et al., 2007). To be Au-rich, the Au content in ppm must exceed the base metal content in weight percent (Gibson et al., 2007). Host rock classification includes five lithological suites which are mafic, bimodal-mafic, bimodal-siliciclastic, bimodal-felsic and siliciclastic-mafic (Galley et al., 2007). Some locations, like an oceanic spreading zone produce mafic volcanic host rock, while felsic is produced at continental arc settings. Bimodal magma occurs in VMS deposits where there were rift developments when the mafic magma rose and blended with the melted felsic crust (Gibson et al., 2007).

In many VMS deposits, sulphide mineralisation commonly occurs as either large concordant sulphide lenses or stringer zones containing discordant veins. The elongated massive sulphide lenses can be up to 100-meters thick, and due to being relatively ductile bodies, they are affected by regional metamorphism and display strain and evidence of recrystallization of the earliest formed sulphide minerals.

The stringers cut through the host rock and connect to the sulphide lenses (Galley et al., 2007).

VMS deposits are actively forming in the present day and are studied around ocean ridges where there is formation of black smokers. These chimneys leach out sulphides that later get deposited in the surrounding host rock and form breccia mounds and eventually form massive sulphide lenses with continued influx of hydrothermal fluids (Galley et al., 2007).

2.2 Au concentration in VMS deposits

The Au-rich deposits are mainly found in calc-alkaline, intermediate to felsic regions commonly associated with arc rifting and subvolcanic intrusions (Dubé and Gosselin et al., 2007). Gold can be found as native metal or together with silver, then forming the alloy electrum. Au can occur in microfractures and inclusions in sulphide minerals as in pyrite and chalcopyrite. The precious metals are most commonly distributed evenly through the sulphide lenses. Au-rich lenses can be found in the same setting as with Au-poor lenses. Therefore, exploration of Au-poor lenses could provide evidence for additional adjacent lenses that might be Au-rich (Dubé and Gosselin et al., 2007).

Depending on the size of lenses or stringer zones, the amount of gold can vary between less than 3 t to more than 300 t Au for a large deposit. If the average Au content in g/t in a VMS deposit exceeds the base metal content in weight percent it is said to be an Au-rich deposit (Dubé and Gosselin et al., 2007).

2.3 Geological setting

The stratigraphy of Westwood is characterised by several mineralized zones of variable extent. The Hébécourt Formation outlines the base of the Westwood deposit, which consists of gabbroic sills and of massive tholeiitic basalt. It is overlain by the Bousquet Formation (2699-2996 Ma) that is divided into two members, the lower is tholeiitic with andesitic to dacitic sills and in contact with the Hébécourt Formation. The strata are overlain by massive andesitic and basaltic lavas. The upper Bousquet member is calc-alkaline in the bottom with andesitic, basaltic and dacitic volcanic rocks, while in the upper layers are more felsic and calc-alkaline with rhyodacitic volcanoclastic rocks. Both members of the Bousquet Formation are affected by synvolcanic intrusions and basaltic to rhyolitic sills and dykes. On top of the Bousquet Formation is turbidites within the Cadillac Group (**Figure 1**) (Yergeau et al., 2015).

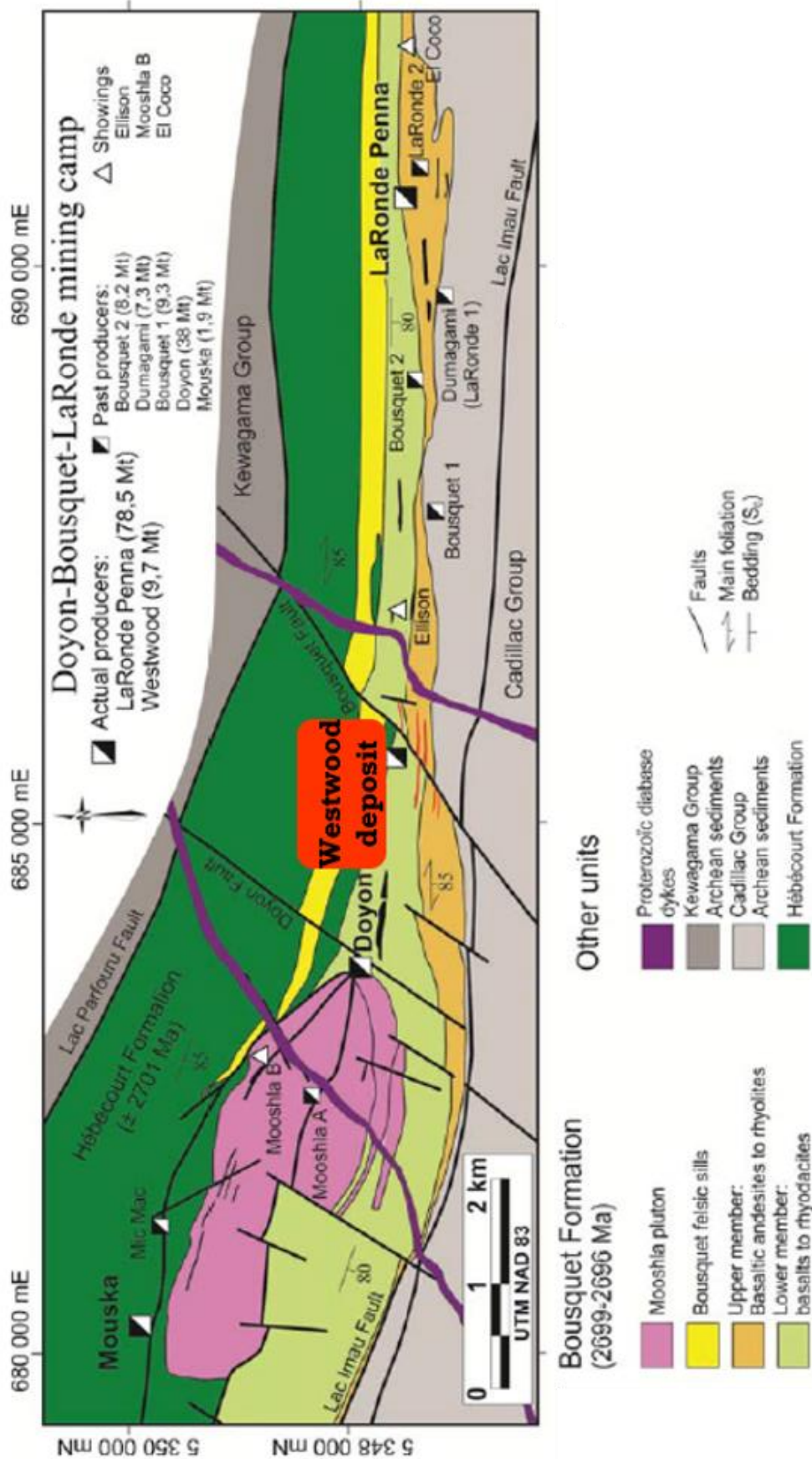


Figure 1. Geological map displaying location of Westwood deposit within Doyon-Bousquet-LaRonde mining camp. Modified from Yergeau et al., 2014.

The area has been affected by regional metamorphism and five deformation events which have given the ore mineralogy and the alteration mineralogy up to lower amphibolite facies and on the retrograde path to upper greenschist facies (Yergeau et al., 2015). The deformation where the ore lenses are found belongs to the major deformation event D2 and a time of shortening in a north-south direction (Yergeau et al., 2015). This caused a stretching in east-west direction and elongated the ore lenses. The following deformation caused cleavages in sericitized rocks, conjugated faults and joints that have contributed to remobilisations of precious and base metals. Deformation event D4 caused formation of faults that produced displacements of up to 3 m for some ore zones. The Westwood deposit is split by the 250 m, subvertical NE-SW, sinistral Bousquet Fault, that formed during the D4 event (Yergeau et al., 2015).

The Westwood ore zones are divided up into three corridors: Zone 2 Extension on the western part of Bousquet Fault, and North Corridor and Westwood Corridor on the eastern part of Bousquet Fault. They are based on the mineralogy and stratigraphy, and have been affected by deformation and strain which has produced stretched ore lenses (**Figure 2**) (Yergeau et al., 2014).

Zone 2 Extension is related to intrusions while North corridor and Westwood corridor are associated with the VMS type of mineralisation. The Zone 2 Extension consist of veins of quartz with large massive sulphide bands (Yergeau et al., 2015). Semi-massive sulphides are disseminated and the major sulphides are pyrite and chalcopyrite, and accessory minerals are sphalerite and pyrrhotite (Yergeau et al., 2015). Pyrite is both early crystallised grains that have endured metamorphism and deformation and later forming pyrites. Felsic sills and dykes are also seen in the Zone 2 Extension in contact with the ore lens.

The North Corridor occurs in the upper member of the Bousquet Formation and is characterised by the minerals pyrite and sphalerite, both as disseminated minerals and located to veins of massive or semi-massive sulphide (Yergeau et

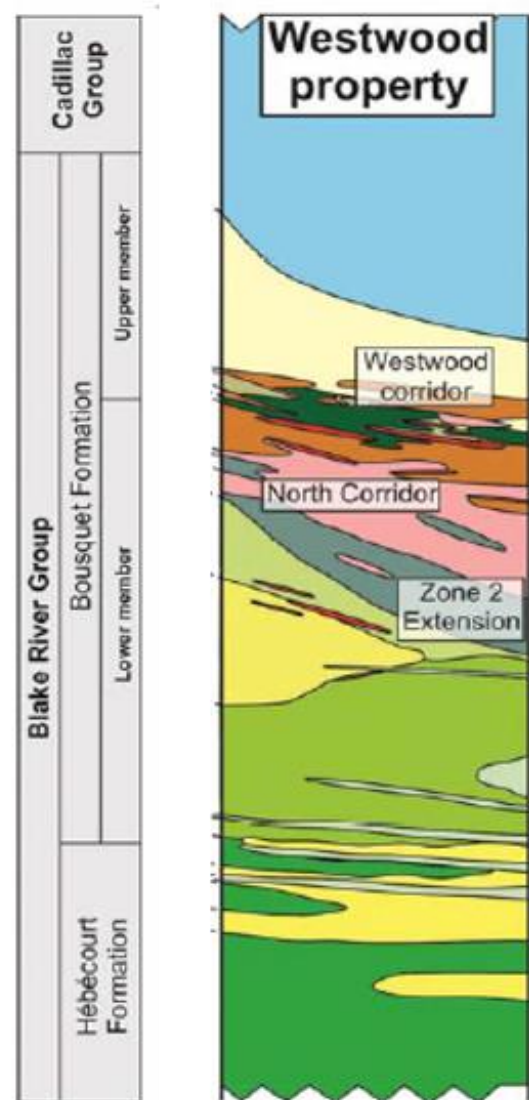


Figure 2. The stratigraphy of Westwood deposit. Not to scale. Modified from Yergeau et al., 2014.

al., 2015). Chalcopyrite, galena and pyrrhotite appear as accessory minerals. The ore zone is affected by deformation and display folding of veins (Yergeau et al., 2015).

The Westwood Corridor (also called Westwood-Warrenmac Corridor) consist of sulphide lenses with distributed sulphide and massive sulphide veins with pyrite and sphalerite, and less abundant galena, chalcopyrite and pyrrhotite (Yergeau et al., 2015). The sulphide lenses are up to 14-metre-thick and the veins are about a metre thick. The Westwood Corridor lies about 100 m above the North Corridor and is also affected by strong deformation that has caused stretching and boudinage formations within the sulphide lenses (Yergeau et al. 2015).

The alteration mineralogy in the Zone 2 Extension consist of altered biotite, chlorite, carbonate and strong sericitization together with quartz. The North Corridor displays sericite together with quartz that are replacing biotite, hornblende, garnet and chlorite. In the upper Westwood Corridor is a stronger assemblage of quartz and sericite that are replacing chlorite, biotite and garnet. The garnets in Westwood Corridor can occur as large porphyroblasts and the abundance in bands of mafic rocks increases closer to the ore zone (Yergeau et al., 2014).

2.4 Au enrichment in Westwood deposit

Canada hosts some of the largest VMS-deposits in the world and Doyon-Bousquet-LaRonde, where Westwood is located, is an important Au-rich deposit with an average grade for Au of 5.35 g/t (Dubé and Gosselin et al., 2007). The Au was calculated to be 3.74 Moz in the Westwood deposit in 2013. The Au is hosted in two types of settings. First is Au-rich VMS deposit and second is associated with intrusions that have given an origin of Au and Cu. Most Au content are related to the synvolcanic event with extensive circulation of hydrothermal fluid and reaction with the magmatic input. All three corridors, Zone 2 Extension, North Corridor and Westwood Corridor have Au that occur as free grains and as the alloy electrum (Au, Ag) within the sulphide lenses (Yergeau et al., 2015). Au also occur as inclusions as very fine grains in recrystallized pyrite and chalcopyrite (Dubé and Gosselin et al., 2007).

3. Methods

The samples were collected from Level 600 (600m depth) by Dr Iain Pitcairn in the summer of 2016. Samples were collected in a section, walking southwards from the Bousquet Fault to intersect two different 2-3m wide VMS horizons. The first VMS horizon is Au-rich, the second being Au-poor. The sampling goes from least altered, with alteration increasing to the VMS horizons and then out to the next horizon, sequentially.

The rocks were cut at Stockholm University and sent to Vancouver Petrographics LTD for further processing into thin sections. One thin section each was made for WE-1 and WE-8. For sample WE-2 to WE-7 there were two sets made, A and B, and it is the set A that is used for SEM and LA-ICP-MS. The thin sections were then used for identification of mineralogy, alteration, and textures by using both reflected and transmitted microscopy. A selection of thin sections were further analysed with SEM and two of these were also examined for trace elements with LA-ICP-MS.

3.1 The SEM

The Scanning Electron Microscope (SEM) was used to confirm identification of minerals in samples WE-2A to WE-7A, since it produces higher magnification than a microscope, and presents information about the chemical composition of minerals. The model of the SEM was a FEG Quanta 650 and the technique is non-destructive. Before analysing in the SEM, the samples were coated with carbon. This was made to prevent the samples from being charged by electrons when analysed, to produce clearer images. Two thin sections at a time were placed in the SEM, and a vacuum was created in the chamber before analysing.

The SEM uses an electron gun to produce a fine beam down to 1 nm in spot size that scans the surface of the thin section in a raster. When the probe touches the surface, it produces secondary electrons and x-rays that are collected by detectors. The signals from the detectors are displayed as black and white images on a computer screen, where the sharpness and contrast can be adjusted for a clearer image (Vernon-Parry, 2000). Any mineral can be analysed and the results are seen on a second computer screen as a spectrum, with the chemical compositions of the minerals and the atomic weight % of each selected spot in the samples. The results from the SEM are qualitative.

3.2 The LA-ICP-MS

For further investigation of minor and trace elements, the Laser Ablation Inductively Coupled Plasma Mass Spectrometry (LA-ICP-MS) was used for the sulphide minerals in the Au-rich sample (WE-6A) and the Au-poor sample (WE-7A). The analysis was performed at Gothenburg University and the model was Quadrupole ICP-MS (Agilent 8800QQQ) with New Wave NWR 213 laser ablation system. The energy output was 2J/cm², repetition rate was 5Hz and helium flow rate was 800 ml/min. The background was measured for 25 seconds and the ablation was 20 seconds, and 20 seconds for it to finish the measurement.

Laser ablation is a technique that is useful for discovering minor and trace elements and isotope ratios (Günther et al., 2005). The samples are put into a vacuumed chamber which contain a carrier gas, in this case it was helium. The laser ablates the thin sections with a narrow beam. The released particles are transferred to the connected ICP-MS which contain a plasma consisting of argon gas. The particles from the laser ablation became vaporised and ionised within the plasma and were further transferred to the mass spectrometer where a detector recognize the separated elements and their masses (Günther et al., 2005).

The isotopes used for the analyses were ^{27}Al , ^{29}Si , ^{34}S , ^{57}Fe , ^{59}Co , ^{60}Ni , ^{63}Cu , ^{66}Zn , ^{75}As , ^{77}Se , ^{95}Mo , ^{107}Ag , ^{121}Sb , ^{125}Te , ^{182}W , ^{197}Au , ^{202}Hg , ^{208}Pb and ^{209}Bi . The spot size was 25 μm and to achieve the most accurate data possible, standards were analysed for calibration after every tenth analysis. The standards were Nist610 (Jochum et al., 2011), GSD, MASS-1 (Wilson et al., 2002), PO725 (Sylvester et al., 2005), AI-3 and MULZnS (Onuk et al., 2016).

The data was processed with the analysing program *Glitter*, where the signals were chosen from the data. The oxide FeO was used as the internal standard for pyrite, pyrrhotite and chalcopyrite, and SO was applied for sphalerite and galena. Data reduction with calibration was made by Johan Högmalm at Gothenburg University. More standards were taken into consideration for this calibration, and this is done instead of normalising the data. The calibration for pyrite, pyrrhotite and chalcopyrite were made of a combination of AI-3, Mass-1, Nist610 and GSD. Mul-1 was set for the calibration of sphalerite. Sulphur was applied as the internal standard for galena, and Mul-1 for calibration.

4. Results and description of samples

4.1 Microscopy

Presented below are descriptions of the samples from Westwood deposit. The results from the SEM and the LA-ICP-MS have aided the identification of mineralogy and alteration processes when they were not able to be identified with the transmitted and reflected microscopy.

WE-1

Lithology: Least altered dacite

Sulphide mineralogy: Pyrite, sphalerite, chalcopyrite and pyrrhotite.

Alteration mineralogy: Quartz, sericite, muscovite, biotite, chlorite and calcite.

Sulphide mineralogy: There is about 10% of opaque minerals in the sample, the most common being pyrite grains. Sphalerite is formed as anhedral grains and as thin needles that have the same orientation and are seen distributed through the whole sample. Pyrites are mostly euhedral and some display caries textures with voids or other minerals as inclusions in the middle of the grains. Pyrrhotite forms small anhedral clusters together with pyrite, and as isolated grains. Chalcopyrite are small patches either surrounded by silicates as single grains or integrated with pyrite and pyrrhotite (**Figure 3**).

Alteration mineralogy: This sample is fine grained silicate rock, with porphyroblastic sulphide minerals. Biotite and chlorite forms between aggregates of sericite. Muscovite is seen stretched and bent around larger porphyroblasts. The sample displays foliation, with strong hydration alteration and sericite throughout the sample. Quartz assembles around the opaque grains. Garnets are euhedral and some have been replaced by chlorite at the edges. Veins of calcite with intergrow quartz crosscuts through the sample.

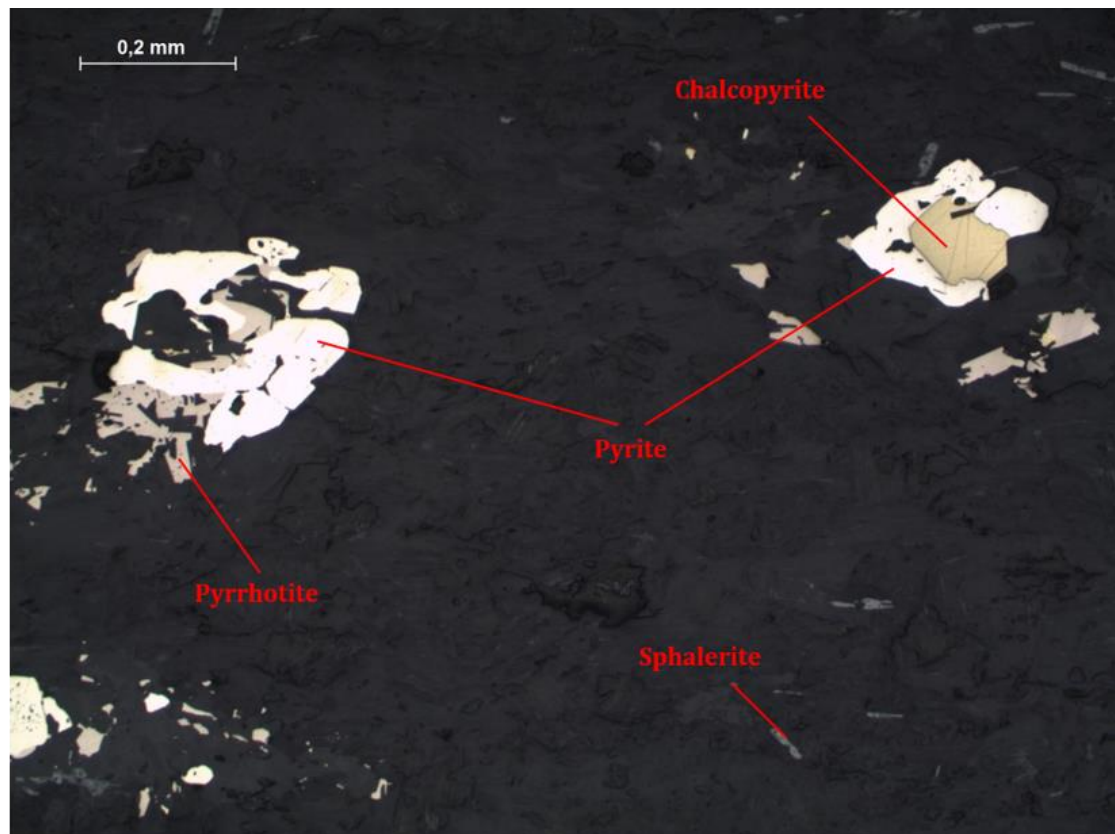


Figure 3. Sulphide porphyroblasts in silicate matrix. Clusters of pyrrhotite, pyrite and chalcopyrite with spherulitic textures.

WE-2

Lithology: Sericite altered basaltic andesite

Sulphide mineralogy: Pyrite, sphalerite and chalcopyrite.

Alteration mineralogy: Quartz, sericite, muscovite, calcite, chlorite, biotite and garnet.

Sulphide mineralogy: This sample consists of about 15% of opaque minerals that are evenly distributed within the altered basaltic andesite (**Figure 4**). There are a few larger porphyroblasts, but most are smaller and evenly distributed in the sample. Pyrites are mostly subhedral, with broken edges and some show caries texture. Chalcopyrite is seen within pyrite as inclusions and in fractures of garnet. Sphalerite occurs as single grains or together with pyrite and chalcopyrite (**Figure 5**). Sphalerite also displays chalcopyrite disease, where the chalcopyrite forms small, rounded inclusions within the sphalerite (**Figure 6**).

Alteration mineralogy: The sample is affected by hydration alteration with sericitization. Veins show foliation of sericite and quartz that is oriented around the opaque minerals. Mica fish around euhedral to subhedral garnet crystals. Vein with calcite have intergrown quartz clusters. Biotite appears as subhedral grains together with chlorite.

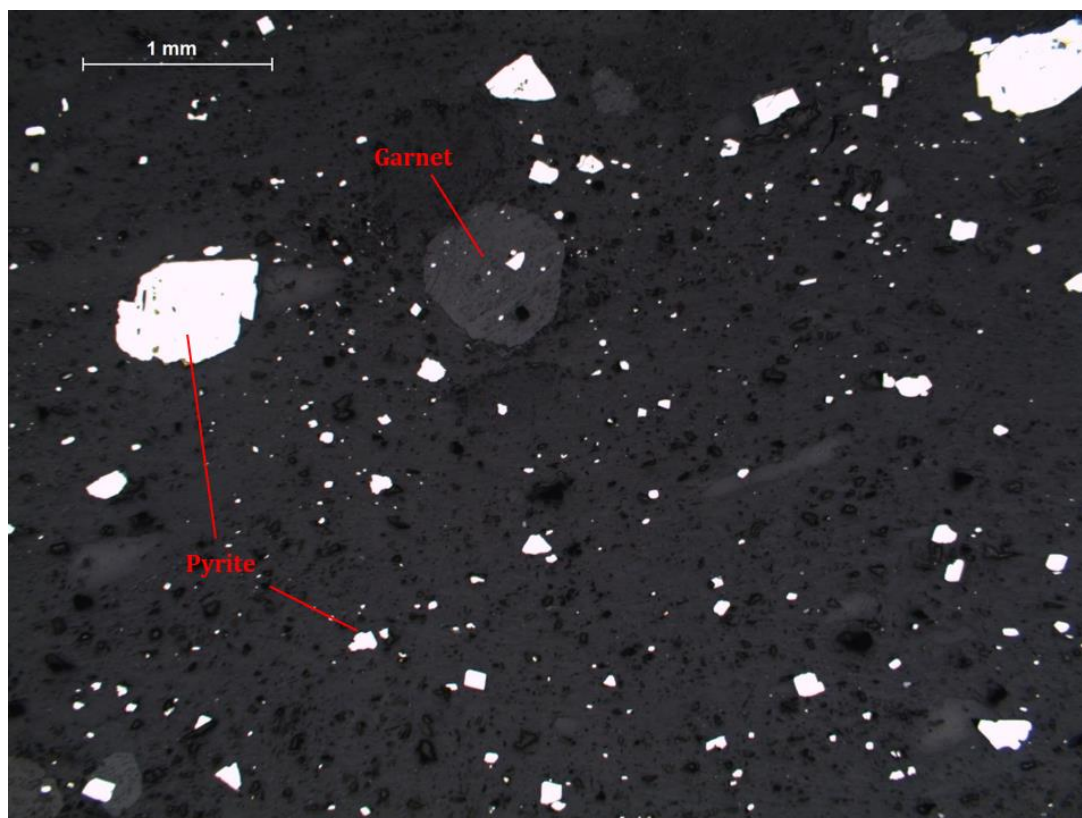


Figure 4. Sulphide grains are evenly distributed in altered basaltic andesite.

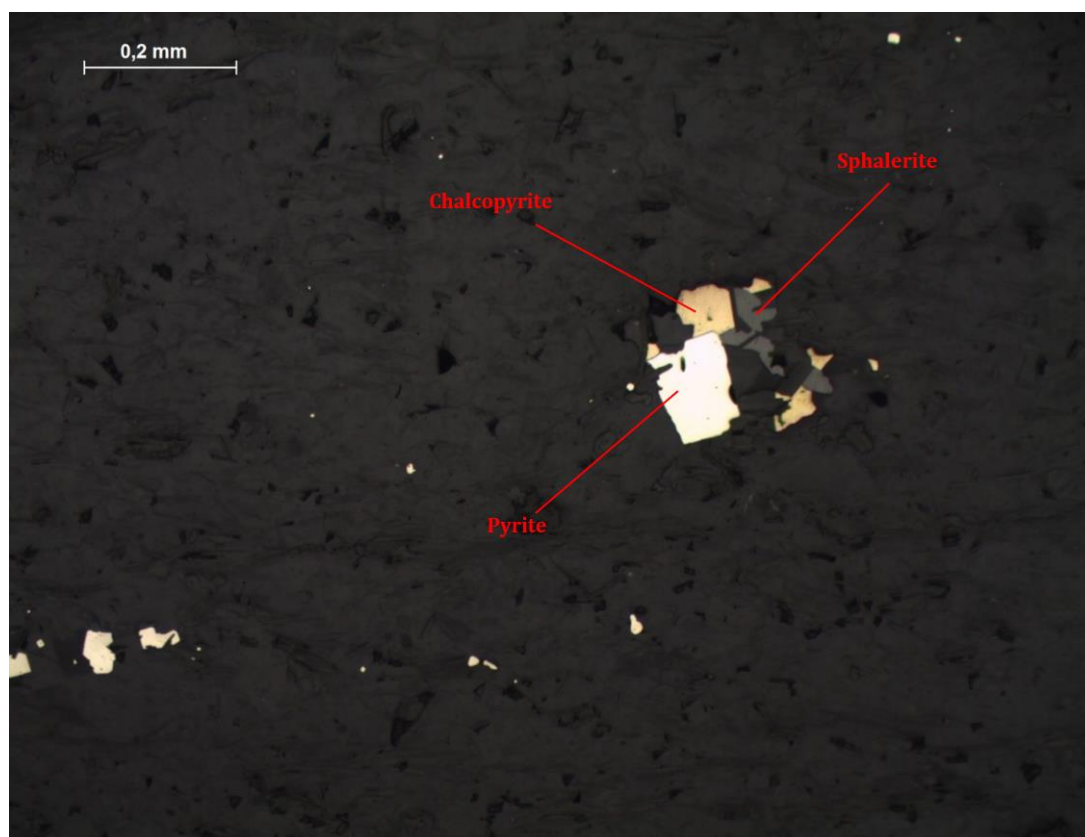


Figure 5. Cluster of pyrite, chalcopyrite and sphalerite in a silicate matrix.

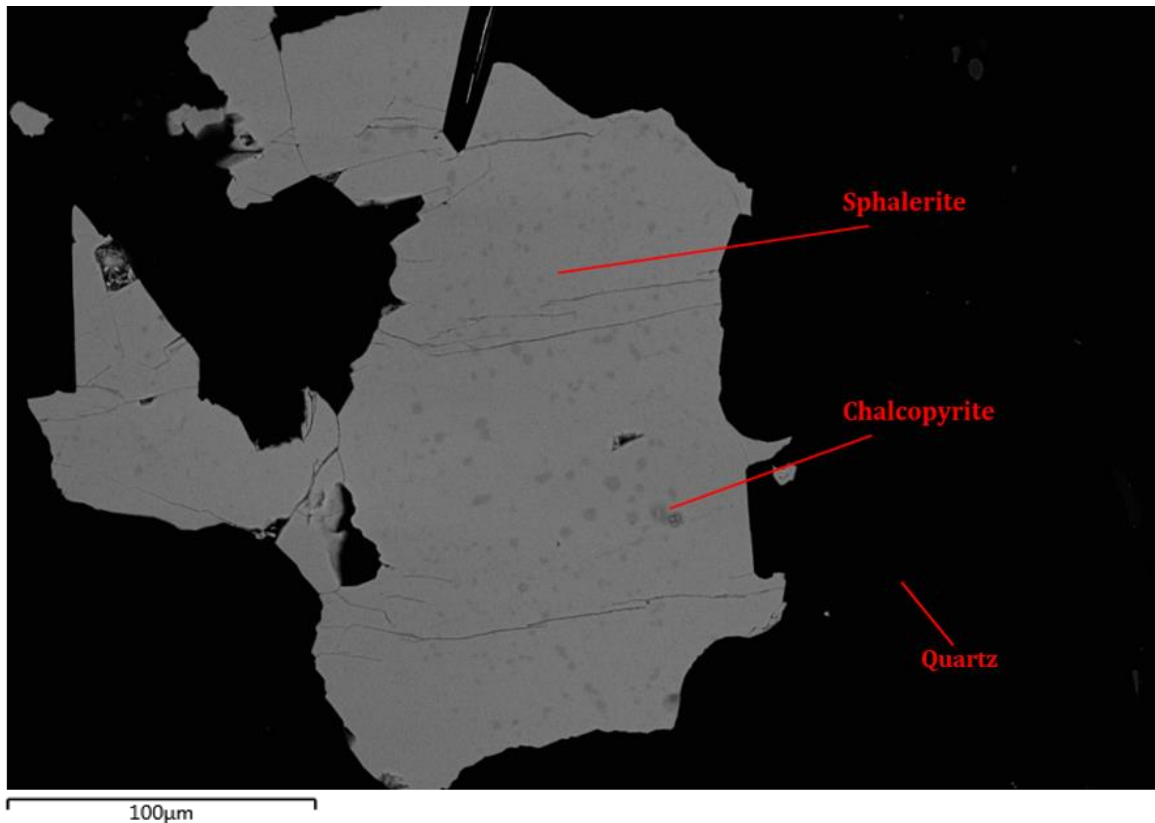


Figure 6. Sphalerite with chalcopyrite disease surrounded by quartz.

WE-3

Lithology: Sericite-pyrite altered dacite

Sulphide mineralogy: Pyrite, sphalerite, chalcopyrite and galena.

Alteration mineralogy: Quartz, muscovite, sericite, calcite, biotite, and garnet.

Sulphide mineralogy: Sample contains about 25% opaque minerals. Sulphide minerals are evenly distributed through the sample and the most abundant mineral is pyrite. Large aggregates of pyrite display inclusions of chalcopyrite and fractures (**Figure 7**). Sphalerite is found as two large anhedral grains with broken edges as well as smaller spots through the sample. Galena appear as inclusions in pyrite or at the pyrite boundary (**Figure 8**).

Alteration mineralogy: Matrix consist mostly of quartz with many small veins of concentrated calcite or sericite. Preferred orientation of mica with the direction of foliation. Larger grains of quartz aggregates around opaque minerals. Minor patches of biotite in the sample together with subhedral garnets that are fractured and replaced by quartz within the fractures.

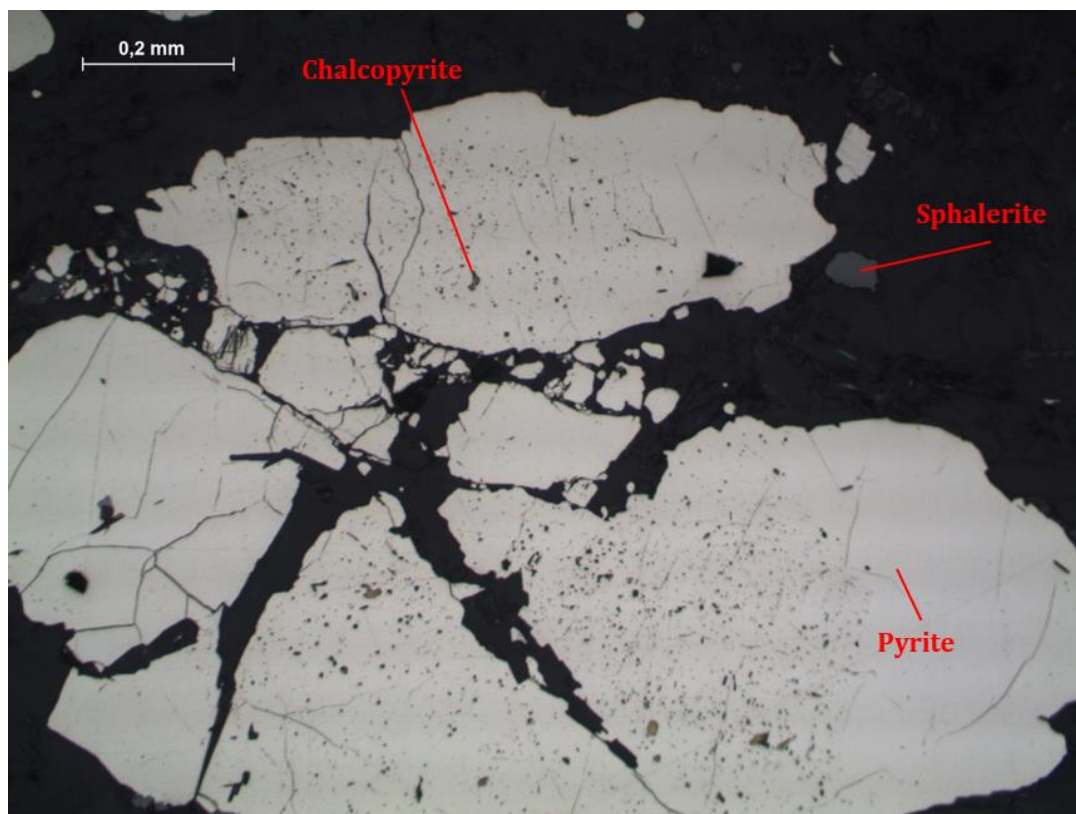


Figure 7. Aggregate of pyrite with inclusions of chalcopyrite, and sphalerite in a matrix of altered dacite.

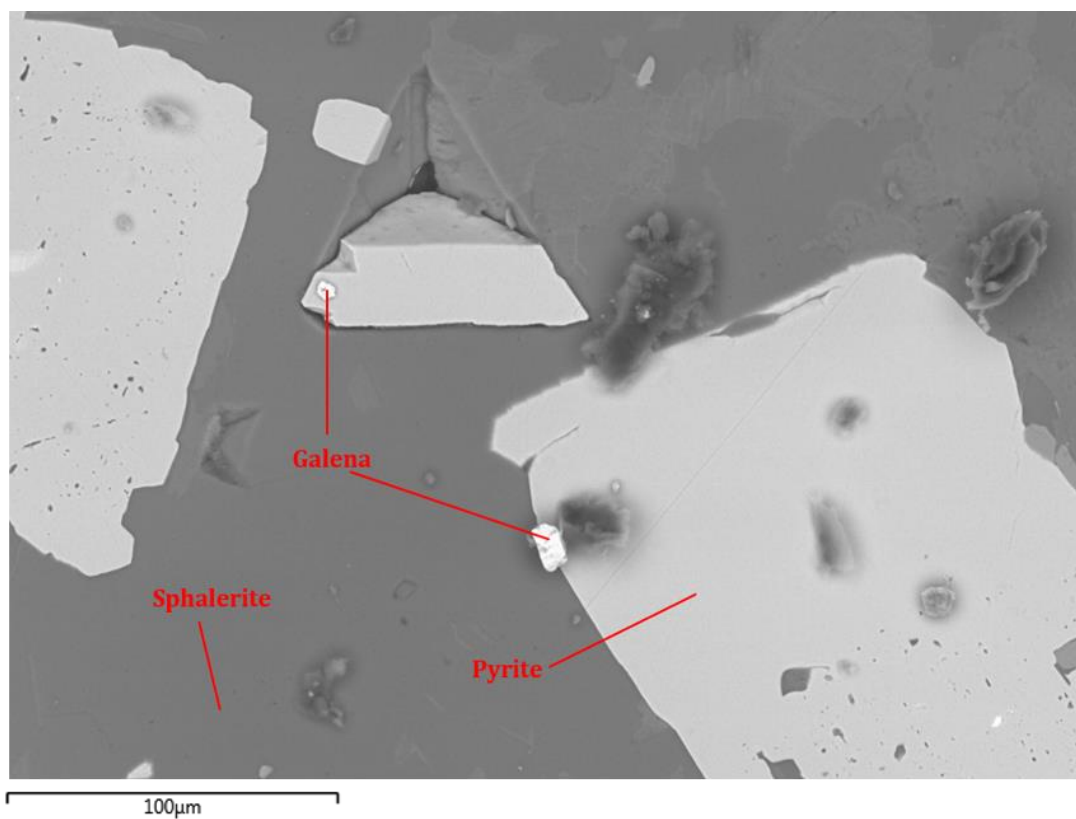


Figure 8. Sphalerite surrounding pyrite with inclusion of galena.

WE-4

Lithology: Stringer zone massive sulphide in dacite

Sulphide mineralogy: Pyrite, sphalerite, chalcopyrite and galena.

Alteration mineralogy: Quartz, sericite, muscovite, calcite, biotite, chlorite and garnet.

Sulphide mineralogy: Sample contain about 40% of opaque minerals. Subhedral to euhedral pyrites are clustered together with thin fractures between the grains that allow chalcopyrite and sphalerite to have grown in them (**Figure 9**). Sphalerite occur also as inclusions within pyrite. Galena forms small veins and anhedral grains between pyrite crystals (**Figure 10**). Chalcopyrite disease is visible within sphalerite as small yellow dots.

Alteration mineralogy: The large opaque porphyroblasts occurs in a matrix consisting of strained quartz and sericite as a result of hydration of the rock. Foliation is seen between the opaque minerals. Large garnet crystals are being replaced by quartz and sericite. Only minor fragments of calcite, chlorite and biotite within the sample.

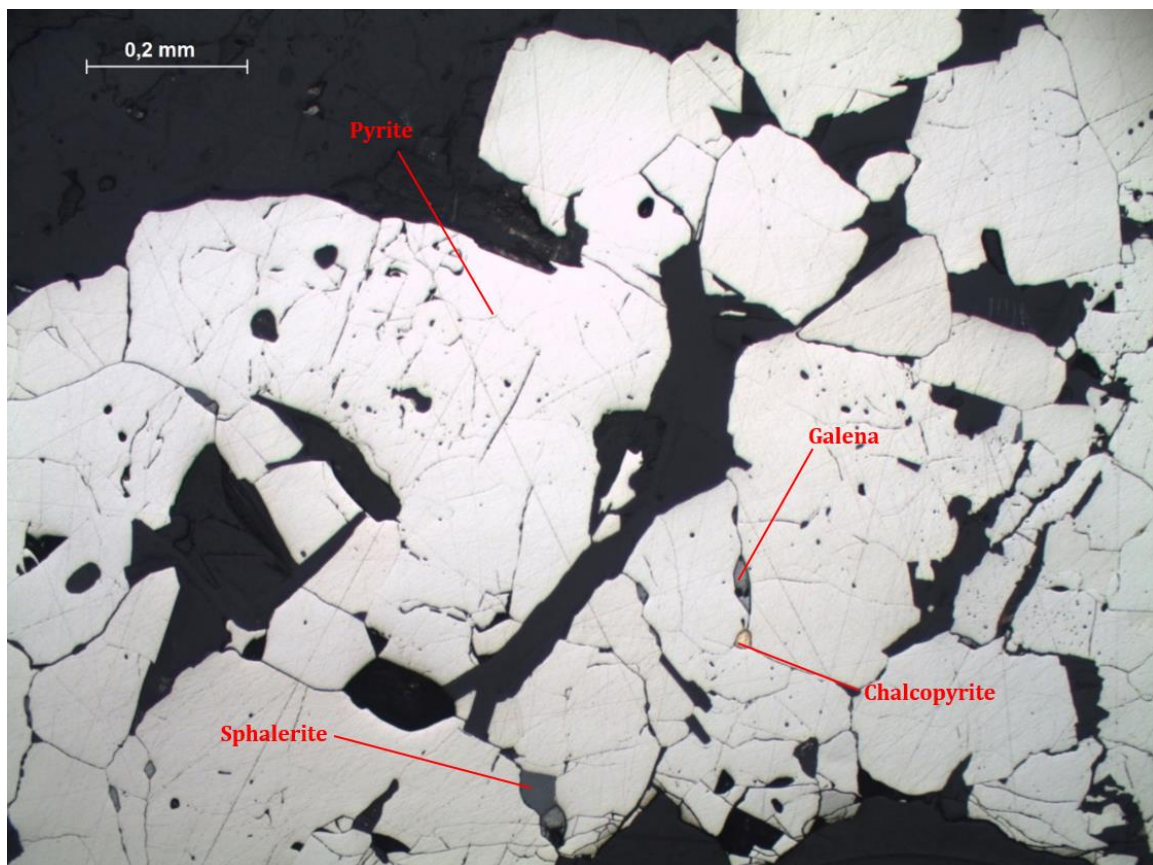


Figure 9. Small patches of chalcopyrite, galena and sphalerite between pyrite aggregate.

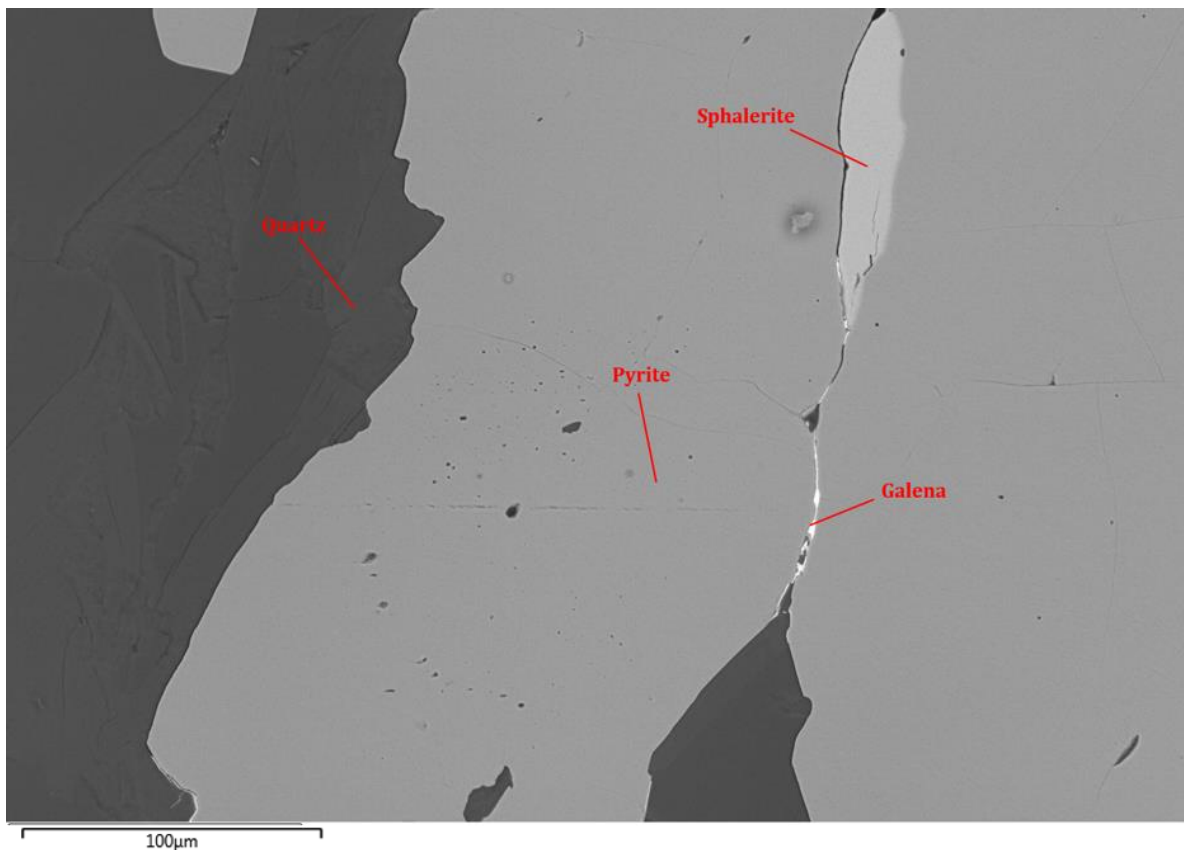


Figure 10. Galena occurring between pyrite grains. Sphalerite forms as a lens between pyrite that contain small inclusions. Quartz occur in contact with pyrite.

WE-5

Lithology: Massive sulphide – banded sphalerite-pyrite. Au-rich.

Sulphide mineralogy: Sphalerite, pyrite, galena, chalcopyrite and pyrrhotite.

Alteration mineralogy: Quartz, muscovite, sericite, calcite and biotite.

Sulphide mineralogy: The sample consist of about 85% of sulphide minerals. The main groundmass is sphalerite. Subhedral to anhedral pyrite grains are either separated as single crystals or consist as aggregates. Pyrites display caries texture (**Figure 11**) with large inclusions of sphalerite and also have fractures (**Figure 12**). Galena and chalcopyrite are small rounded inclusions within pyrite but galena also occur in sphalerite (**Figure 13**). Only few minor inclusions of pyrrhotite that occur within pyrite grains.

Alteration mineralogy: Only small part of silicate minerals that occur between the opaque grains. Veins of clustered quartz with elongated muscovite and biotite between sulphide minerals. Sericite is in contact with quartz vein. Calcite appear as single grains.

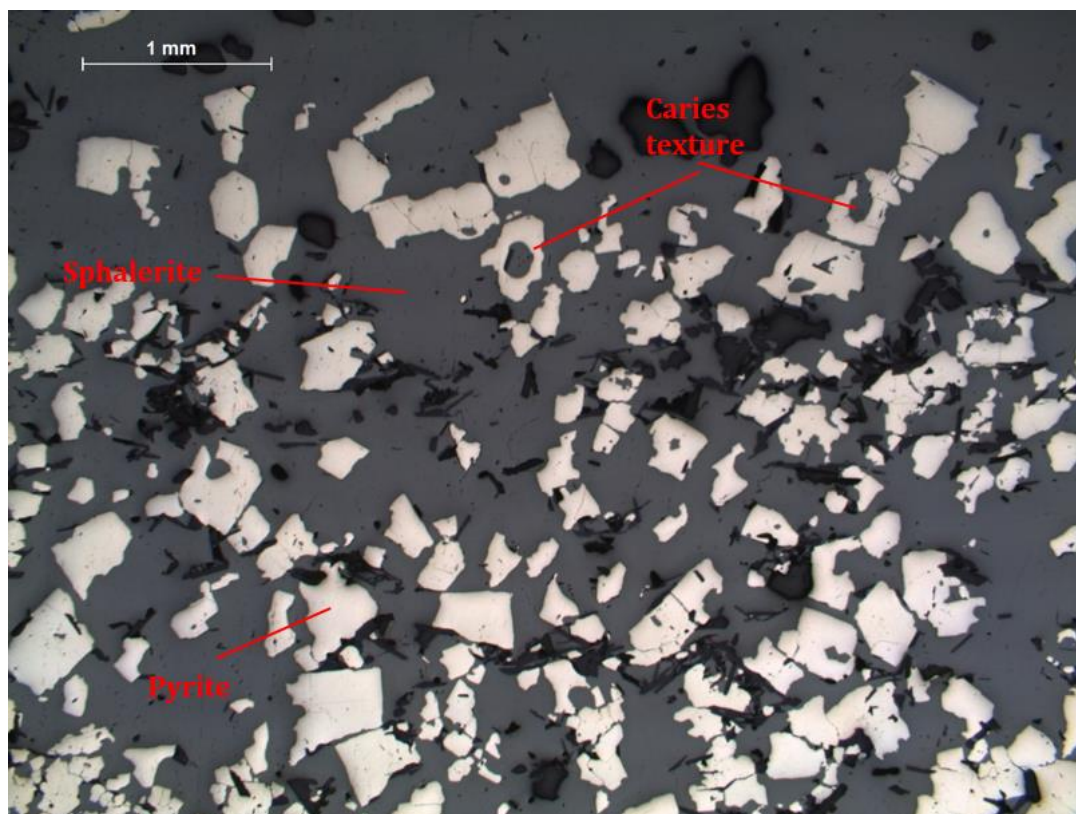


Figure 11. Evenly distributed pyrite in sphalerite matrix. Pyrite display caries texture, large holes within or at edges of the grains.

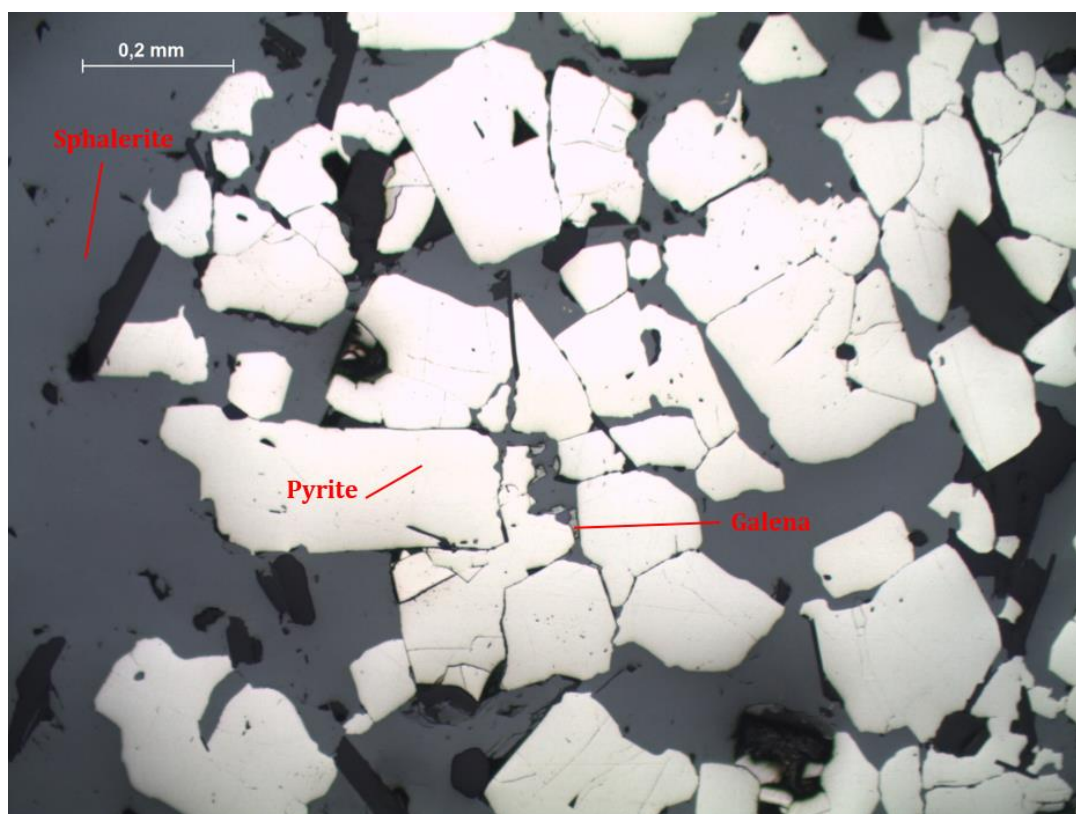


Figure 12. Pyrite surrounded by sphalerite and small galena patches in the sphalerite.

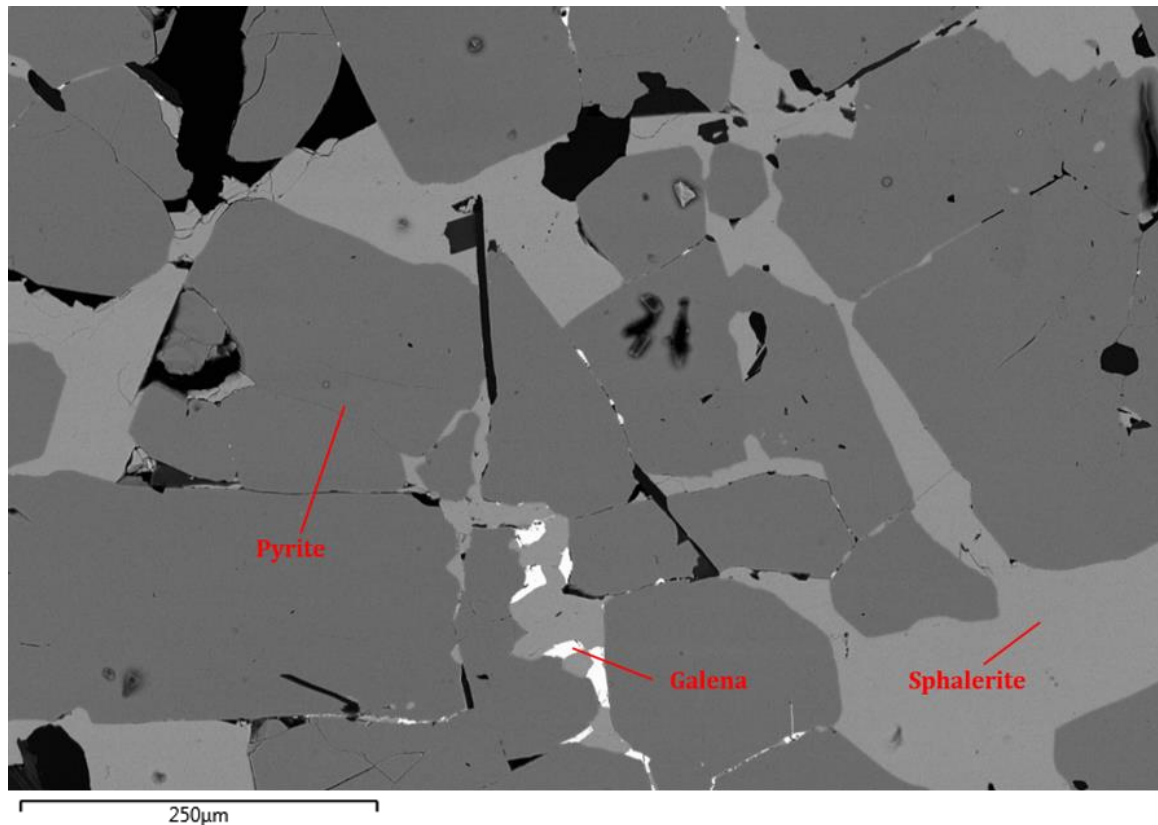


Figure 13. Pyrite crystals with light grey sphalerite between. Bright grains are galena seen in sphalerite.

WE-6

Lithology: Massive sulphide – banded sphalerite-pyrite ore with quartz lens. Au-rich.

Sulphide mineralogy: Sphalerite, pyrite, chalcopyrite, pyrrhotite, galena and electrum.

Alteration mineralogy: Quartz, muscovite, sericite, calcite, biotite and chlorite.

Sulphide mineralogy: The opaque minerals comprise of about 80% of the sample. Euhedral to subhedral pyrite grains in a groundmass consisting of sphalerite. Pyrites shows caries texture and some grains display many inclusions, mostly in the centre of the crystals. Sphalerite occur as inclusion in pyrite. Chalcopyrite is seen in sphalerite as chalcopyrite disease and as smaller aggregates. Pyrrhotite forms large irregular aggregates between the other minerals (**Figure 14**). Galena and electrum are seen only as minor grains between the major minerals (**Figure 15**).

Alteration mineralogy: Alteration minerals are distributed between the sulphide minerals and as a large aggregate in the corner of the sample consisting of quartz and calcite that occur as small veins. Muscovite and sericite are unevenly oriented between the sulphide minerals. Biotite and chlorite are in disequilibrium and displays broken fragments.

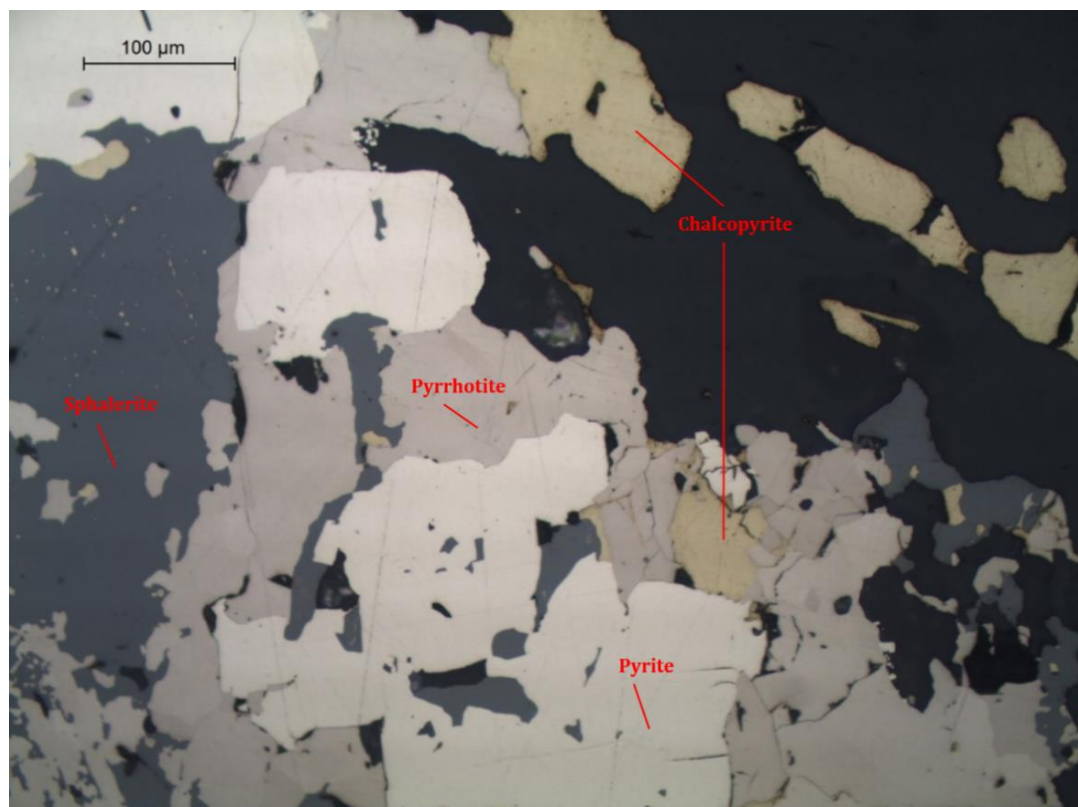


Figure 14. Pyrrhotite, pyrite, chalcopyrite together with silicates. Chalcopyrite disease in sphalerite.

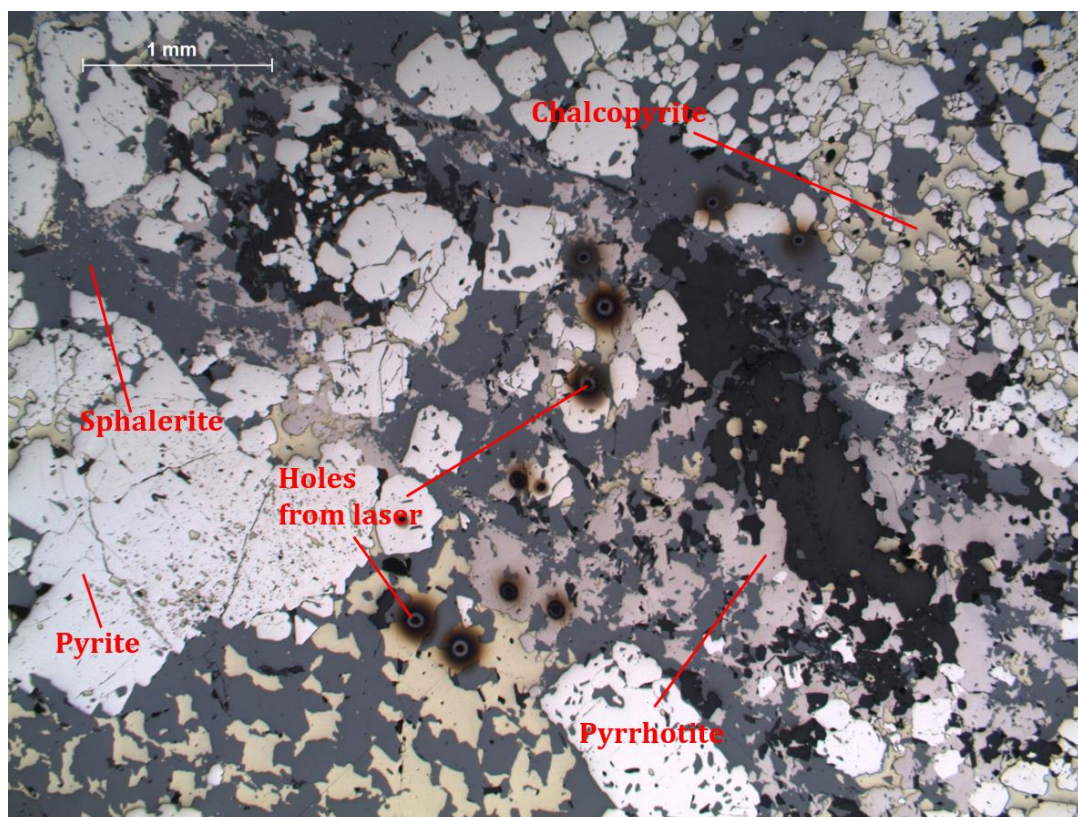


Figure 15. Distribution of recrystallized pyrite, intergrown pyrrhotite and chalcopyrite together with sphalerite. Dark spots are holes from laser ablation.

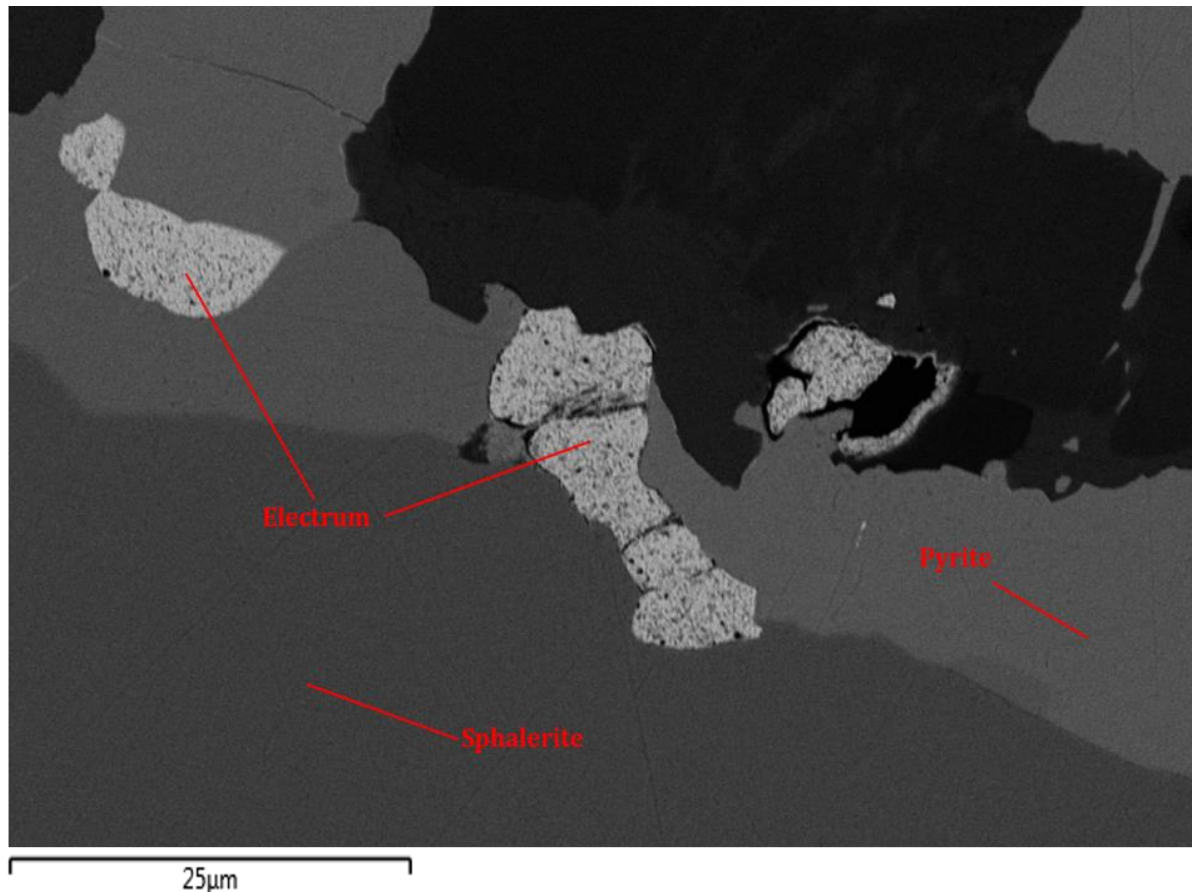


Figure 16. Au, Ag alloy (electrum) in pyrite together with sphalerite.

WE-7

Lithology: Massive sulphide – pyrite-rich. Au-poor.

Sulphide mineralogy: Pyrite, sphalerite, chalcopyrite and galena.

Alteration mineralogy: Quartz, muscovite and calcite.

Sulphide mineralogy: Sample consist of about 95% of sulphide minerals. Mostly monomineralic sample that mainly consist of massive pyrite. Compacted pyrite crystals that have intergrown with each other. Pyrites are euhedral to subhedral and contain some inclusions but not in the same amount as within WE-6 (**Figure 17**). Chalcopyrite, sphalerite and galena occur in the voids between pyrite (**Figure 18**). Galena forms as lens-shaped bodies and appears in thin veins between the pyrite crystals (**Figure 19**).

Alteration mineralogy: Only minor parts of silicates in the sample that locates between the large sulphide crystals. Vein of aggregated quartz and calcite cuts through the sulphides. Muscovite occurs as small needles through the whole sample without any preferred direction of orientation.

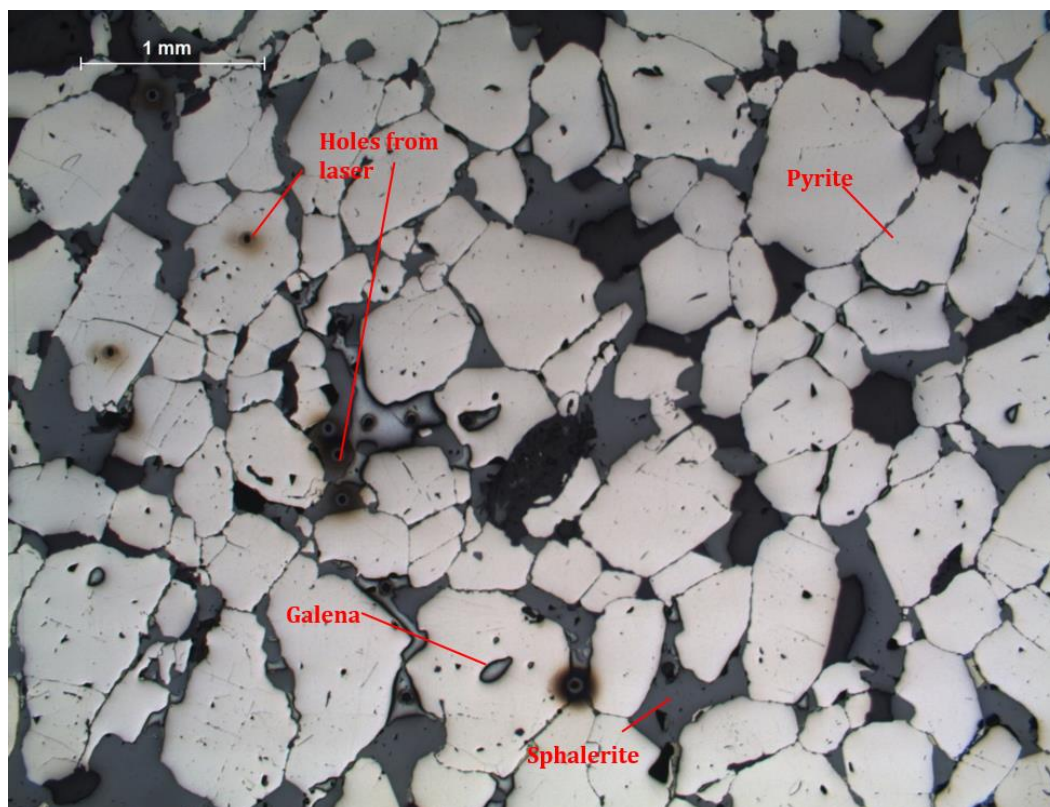


Figure 17. Massive intergrown pyrite with sphalerite and galena filling the voids between the pyrite. Dark rounded spots are holes from laser ablation.

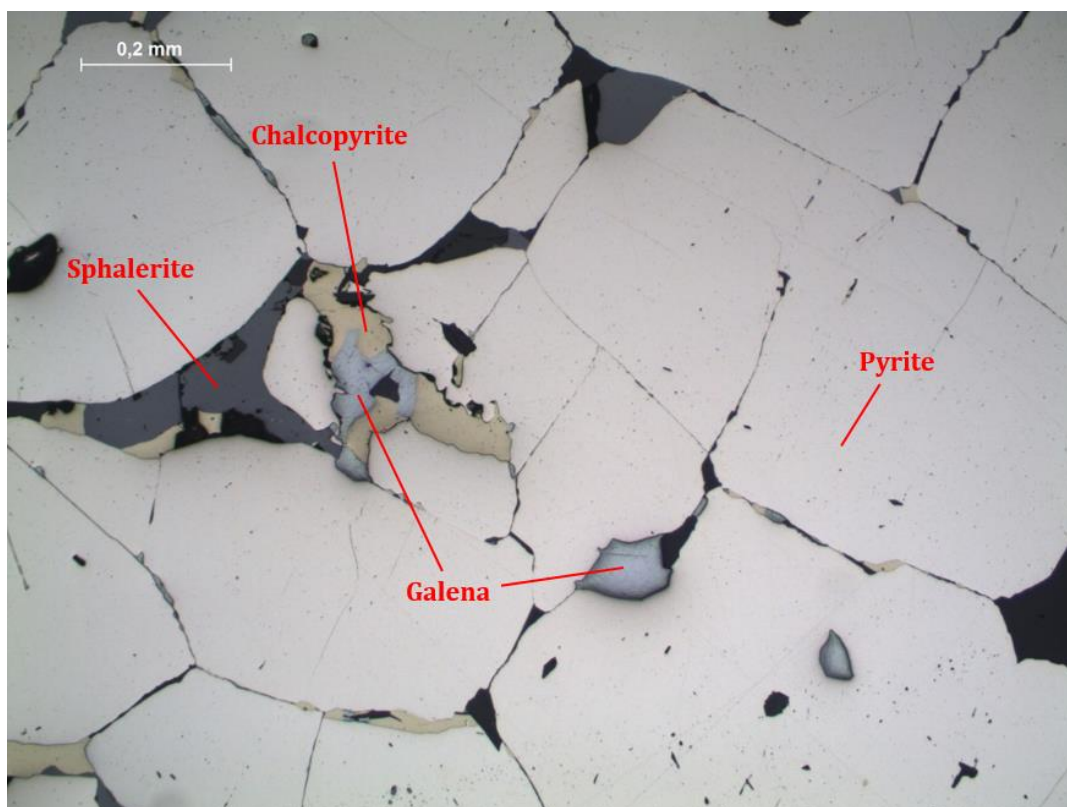


Figure 18. Cluster of intergrown pyrite crystals with chalcopyrite, galena and sphalerite between.

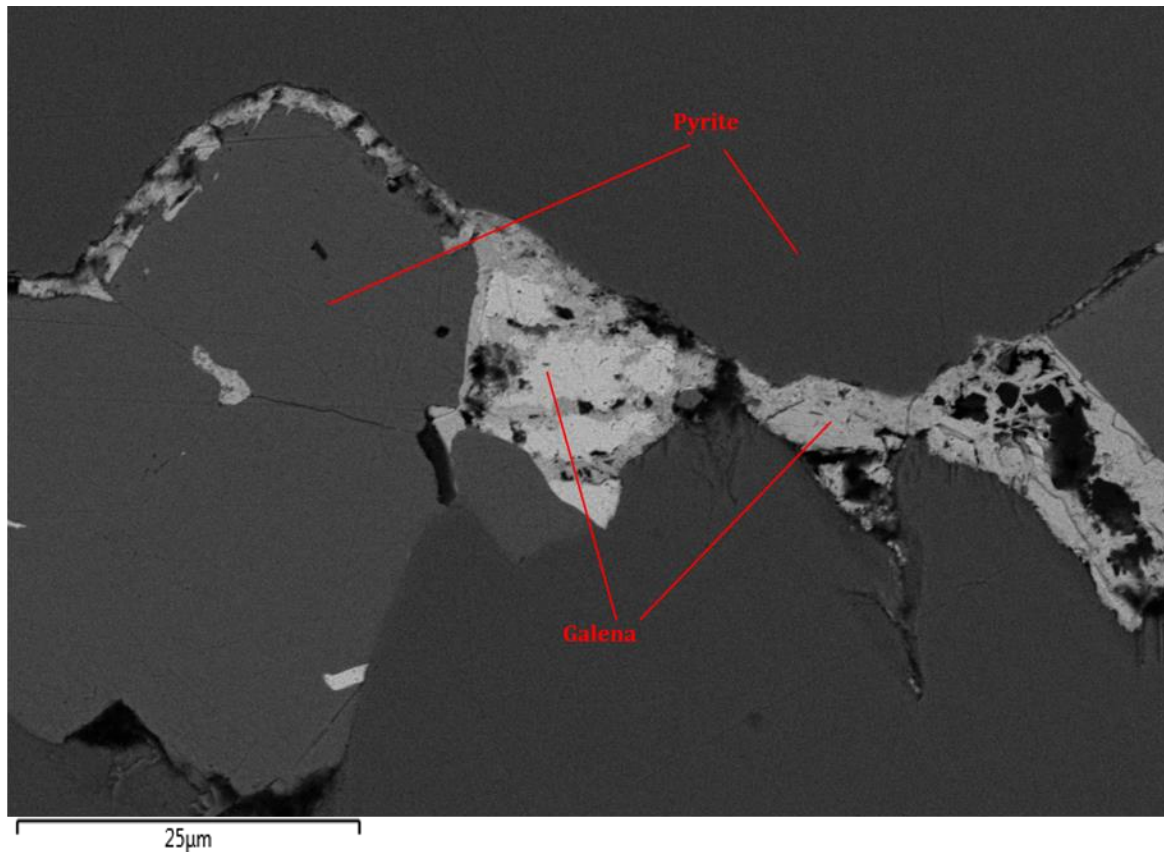


Figure 19. Small vein with galena between pyrite crystals.

WE-8

Lithology: Least altered dacite above ore lens

Sulphide mineralogy: Pyrite, sphalerite and chalcopyrite.

Alteration mineralogy: Quartz, sericite, muscovite and calcite.

Sulphide mineralogy: The sample contains about 5% of sulphide minerals. Small porphyroblasts of pyrite and sphalerite within a matrix of silicate minerals. The pyrites are subhedral with inclusions and holes and in contact with patches of chalcopyrite. Pyrite form small elongated aggregates in the same direction as foliation in the sample (**figure 20**). Sphalerites exhibit skeletal structure and are in disequilibrium.

Alteration mineralogy: Fine grained metamorphosed sample with some porphyroblasts of sulphide minerals. Shows foliation and a preferred orientation of direction for the muscovite. Calcite is located to veins together with quartz. Mica surrounds aggregates of quartz and sericite is distributed evenly through the complete sample.

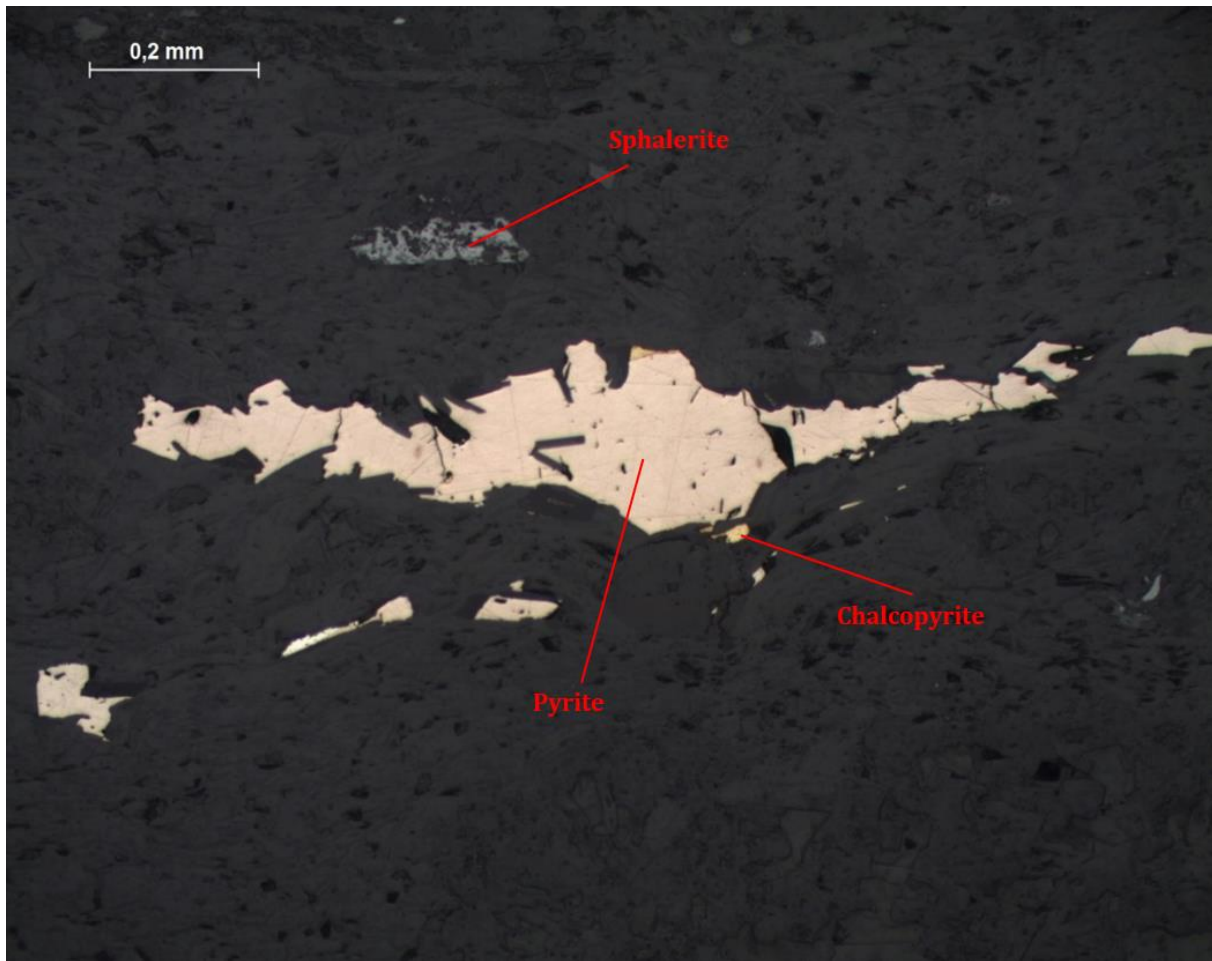


Figure 20. Pyrite aggregate with chalcopyrite and sphalerite in silicate matrix.

4.2 SEM results

The analyses from SEM displays as spectrums for each mineral and its chemical composition in atomic weight %. Analyses are for the sulphide minerals within samples WE-2A to WE-7A. Results are qualitative and are shown in **Table 2**.

The mineralogy and textures are seen in black and white images, with higher magnification than what could be achieved with the microscope. The presented results illustrate the average value and standard deviation for pyrite, sphalerite, chalcopyrite, pyrrhotite, galena, silver and gold.

Au and Ag are only seen present in WE-5 and WE-6 that are collected from the Au-rich location of Westwood. These metals form the alloy electrum. For WE-5 the average Au is 44.78, which is higher than Ag that is 13.82 atomic weight %. In WE-6 the amount of Ag exceeds the amount for Au. The average is 10.11 for Au and 74.45 atomic weight % for Ag.

Table 2. Results from the SEM (All values are in atomic weight %)								
Sample	WE-2A							
Mineral	<u>Pyrite</u>		<u>Sphalerite</u>		<u>Chalocpyrite</u>			
Element	<i>Fe</i>	<i>S</i>	<i>Zn</i>	<i>S</i>	<i>Cu</i>	<i>Fe</i>	<i>S</i>	
	34,8	65	48,8	46,9	26,3	27,8	44,3	
	34,9	65,1	48,6	46,3	25,1	27,5	47,2	
	29,7	58,9			25,3	27,5	47,2	
					24,6	26,1	47	
					23,1	23,1	47,7	
Average	33,13	63,00	48,70	46,60	24,88	26,40	46,68	
StDev	2,97	3,55	0,14	0,42	1,17	1,96	1,36	
Sample	WE-3A		WE-4A					
Mineral	<u>Pyrite</u>		<u>Pyrite</u>		<u>Sphalerite</u>		<u>Galena</u>	
Element	<i>Fe</i>	<i>S</i>	<i>Fe</i>	<i>S</i>	<i>Zn</i>	<i>S</i>	<i>Pb</i>	<i>S</i>
	34,6	65,4	34,8	65,2	49,7	46,7	25,1	33,8
	33,8	62,5	27,4	50,3			30,7	47,7
	34,7	65,3	34,5	65,5				
	34,5	65,2						
Average	34,40	64,60	32,23	60,33	49,70	46,70	27,90	40,75
StDev	0,41	1,40	4,19	8,69			3,96	9,83
Sample	WE-5A							
Mineral	<u>Pyrite</u>		<u>Sphalerite</u>		<u>Galena</u>		<u>Gold</u>	<u>Silver</u>
Element	<i>Fe</i>	<i>S</i>	<i>Zn</i>	<i>S</i>	<i>Pb</i>	<i>S</i>	<i>Au</i>	<i>Ag</i>
	34,4	65,6	47,5	46,6	43,7	43,4	65,9	14,5
	34,1	65,4	48,8	46,5	43,5	43,4	57,7	18,7
	34,6	65,4	48,8	46,6	42,3	42	4,8	0,8
	34,6	65,4	47,4	47,2	39,2	45,1	42,4	13,8
	33,4	66,1	44,9	47,8	44,1	45	27,2	13,4
	34,4	65,6	46,1	46,3	47,5	47,4	70,7	21,7
	34,3	65,3	48,5	47,4	17,6	40,2		
	34,4	65,6	47,8	47	32,5	47,8		
	34,7	65,3	47,6	47	33,3	41,7		
	34,4	65,6	48,9	47,1	40,6	41,8		
	34,5	65,1	46,8	47,8	44,2	43		
	38,8	60,6			25,7	27,7		
	34,4	65,6			41,5	41,7		
	34,4	65,6			40,8	38,2		
	34,5	65,5			42,2	41,9		
	34,4	65,6			42	41,6		
	19,4	75,9			46,7	46,3		
	34,3	65,7						
Average	33,78	65,83	47,55	47,03	39,26	42,25	44,78	13,82
StDev	3,75	2,78	1,25	0,50	7,82	4,52	25,29	7,16

Sample	WE-6A										
Mineral	Pyrite		Sphalerite		Chalcopyrite			Pyrrhotite		Gold	Silver
Element	Fe	S	Zn	S	Cu	Fe	S	Fe	S	Au	Ag
	32,8	67,2	48,2	46,1	29,5	23,8	46,7	50	50	1,6	81,9
	34,9	65,1	42,5	45,7	39,1	23	46,9	48,6	51,4	9,7	51,3
	33,5	66,5	48	43,6	28,9	26,9	44,2	48,5	51,5	9,9	92,4
	28,9	48,7	44,4	42,5	29,5	21,5	48,9	45,3	54,7	11,7	89,2
	34,3	65,7	36,5	48,3	29,4	23,9	46,7	45,5	54,5	6	100
	32,5	67,5	49,8	45	29,6	25,1	45,3	48,7	51,3	12,4	96,5
	33,3	66,7	40,8	43,4	29,7	25,9	44,4	45,5	54,5	10,2	90,3
	34,4	65,6	50,5	49,5	30,1	23,9	46	46,3	53,7	11	80,5
	33,6	66,4	50,6	44,8	29,7	22,2	48,1	48,7	51,3	10,7	82,1
	32,6	67,4	42,8	45,3	25,3	22,9	51,7	46,7	53,3	8,9	44,6
	32,3	67,7	41,2	42,9	29,9	22,7	47,4	48,4	51,6	12,4	81,3
	32,4	67,6	48,8	46,9	29,6	22,8	47,5	48,3	51,7	12,4	84,1
	33,9	66,1	42,1	43	18,9	30,4	50,6	50,2	49,8	7,2	83,8
	35,3	64,7	48,6	45,6	28,9	22,1	49,1	46,4	53,6	9,1	81,9
	34,1	65,9	49,3	48,5	30,1	24,6	45,4	48	52	5,2	91,1
	29,9	55,4	42,8	44,7	29	24,2	46,8	47,6	52,4	9,3	80,4
	32,6	67,4	45,2	45,3	29	25,1	45,9			13,5	87,6
	31	69	43,7	45,3	29,5	22,9	47,6			13	50,2
	32,8	67,2	48,8	46,3	30,6	22,8	46,6			11	61,3
	33,8	66,2	52,5	47,5	23,4	29,2	47,4			12,7	43,1
	34,9	65,1	43,7	44,8	30,4	23,4	46,2			13,8	7,4
	33,5	66,5	50	50	30,4	22	47,6			10,7	97,4
	34,2	65,8	48,5	45,3	29,3	22,1	48,5				68,6
	35,9	64,1	48,7	45,5	31,1	19,6	49,3				15,4
	32,1	67,9	42,8	43,2	30,3	24,6	45,2				85,3
	34,3	65,7	43,9	42,7	29,6	22,7	47,7				72,8
	33,6	66,4	40,6	41,3	29,1	25,1	45,8				79,3
	36	64	43,6	42,4	29,7	23,6	46,7				76,2
	35,9	64,1	48,7	45,5							87,3
	33,4	66,6	49,5	45,9							81,7
	36,1	63,9	42,2	43,3							83,1
	35,5	64,5	43,5	42,1							
	31,9	68,1	41,6	44,6							
	32,3	67,7	48,7	44,6							
	33,5	66,5	50,9	48							
	33	67	43,9	37,5							
			42,7	45,6							
			43,8	42,5							
Average	33,47	65,50	45,64	44,87	29,27	23,89	47,15	47,67	52,33	10,11	74,45
StDev	1,62	3,63	3,78	2,41	3,14	2,23	1,73	1,55	1,55	2,98	22,36

Sample	WE-7A								
Mineral	Pyrite		Sphalerite		Chalcopyrite			Galena	
Element	Fe	S	Zn	S	Cu	Fe	S	Pb	S
	33,5	66,5	43,4	44,8	29,7	24,5	45,8	54,4	45,6
	34,7	65,3	50,3	47,3	30,2	22,6	47,2	25,3	18,7
	33,2	66,8	49,2	45,4	30,3	22,2	47,4	57	43
	34,7	65,3	52,5	47,5	30,3	24,2	45,6	56	44
	34,9	65,1	43,3	44,2	29,7	23,8	46,5	53	47
	32,3	67,7	51,3	46,3	31,1	21,6	47,3	56	44
	32,4	67,6	50,2	44,3	29,7	25,6	44,7	55,2	44,8
	34,2	65,8	44,6	42	28,4	25	46,6	53,2	46,8
	32,5	67,5	52,6	46,4	33,3	24	45,7	21	13,3
	33,9	66,1	50,5	44,6	29,8	24,4	45,8	56,3	43,7
	33,7	66,3	51,	49	30,7	24,8	44,6	46,1	40,4
	33,7	66,3			30	23,4	46,6	55,8	44,2
	32,1	67,9			30,2	24,8	45	20,5	13,7
					30,7	20,1	49,1	23	11,2
								52,5	47,5
Average	33,52	66,48	48,99	45,62	30,29	23,64	46,28	45,69	36,53
StDev	0,97	0,97	3,51	1,94	1,07	1,52	1,23	14,77	14,10

4.3 LA-ICP-MS results

The results from the LA-ICP-MS are presented below with concentrations in ppm for each element and mineral. The samples represent each spot analysed with sample name (WE-6A or WE-7A), the number of the analyse, reference to SEM photo with a letter, and shortening for the mineral that were analysed. All cursive zeros represent values below detection limit. The values for detection limit is based on Nist610 for 25 micron spots (**Table 3**).

Some of the isotopes were excluded and presented below are the relevant isotopes for this study. They are ^{75}As , ^{77}Se , ^{95}Mo , ^{107}Ag , ^{121}Sb , ^{125}Te , ^{182}W , ^{197}Au and ^{209}Bi . The results in **Table 4** are compiled to display the calculated average, standard deviation and minimum and maximum values for each element of the ablated spot.

Table 3. Detection limits based on Nist610 for 25 micron spots.

Detection limits	As75	Se77	Mo95	Ag107	Sb121	Te125	W182	Au197	Bi209
	0,5	1,5	0,4	0,06	0,2	0,4	0,01	0,03	0,06

Table 4. Results from LA-ICP-MS (All values are in ppm)									
Sample	Element								
<u>Pyrite</u>	<u>As75</u>	<u>Se77</u>	<u>Mo95</u>	<u>Ag107</u>	<u>Sb121</u>	<u>Te125</u>	<u>W182</u>	<u>Au197</u>	<u>Bi209</u>
WE-6A-2-P-PY	0,342	95,7	0,335	288	0,156	1,114	0	0	0,074
WE-6A-3-P-PY	0	97,1	0,201	255	0,407	0,158	0	0	0,010
WE-6A-4-A-PY	66,4	10,3	0	0,404	0,620	0,108	0	0,005	0,013
WE-6A-9-0-PY	38,3	18,1	0,131	0,128	0,104	0,077	0	0,007	0,001
WE-6A-11-B-PY	324	10,8	0,026	0,005	0,015	0,072	0	0	0
WE-6A-13-C-PY	610	9,18	0,055	0,077	0,131	0	0,004	0,022	0
WE-6A-15-L-PY	326	10,1	0,258	44,6	6,596	0,093	0,021	0,057	0,087
WE-6A-18-K-PY	301	10,1	0,042	0,068	0,026	0,051	0	0,005	0,019
WE-6A-26-M-PY	36,7	25,3	0	0,502	0,692	1,286	0	0	0,004
WE-6A-32-N-PY	357	13,5	0,119	0,004	0	0	0	0,011	0
WE-6A-41-H-PY	405	10,2	0	0,372	0,623	0	0	0,005	0
WE-6A-43-H-PY	70,3	10,5	0,075	0,010	0,012	0	0	0	0,007
Average	211	26,7	0,104	49,0	0,78	0,25	0,002	0,009	0,018
StDev	200	32,9	0,110	105	1,85	0,45	0,006	0,016	0,030
Maximum	610	97,1	0,335	288	6,60	1,29	0,021	0,057	0,087
Minimum	0	9,18	0	0,004	0	0	0	0	0
Pyrrhotite									
<u>Pyrrhotite</u>	<u>As75</u>	<u>Se77</u>	<u>Mo95</u>	<u>Ag107</u>	<u>Sb121</u>	<u>Te125</u>	<u>W182</u>	<u>Au197</u>	<u>Bi209</u>
WE-6A-7-A-PO	0	35,6	0	2,98	0	0	0	0,013	0
WE-6A-8-0-PO	0,003	43,4	0	2,38	0,185	0	0	0,007	0
WE-6A-12-B-PO	0	40,7	0,065	189	0,765	0	0,010	0,141	0
WE-6A-21-G-PO	0,473	35,9	0	70,0	4,22	0,037	0	0	0,036
WE-6A-23-G-PO	0,802	38,8	0,239	3753	0,946	0,037	0,111	0	0
WE-6A-29-N-PO	0	54,1	0	489	0,541	0,056	0	1,35	0
WE-6A-30-N-PO	0	159	0	1843	2,69	0,949	0	0	0,044
WE-6A-35-N-PO	0	43,4	0	63,4	0,419	0	0	1,56	0,019
WE-6A-36-N-PO	0,063	43,6	6,33	171	3,02	0	0,562	3,30	0
WE-6A-42-H-PO	0	48,2	0,226	5,01	0	0,085	0	0	0
WE-6A-46-H-PO	0,025	49,2	0	3,56	0,073	0	0,096	0,012	0
WE-6A-47-H-PO	0,109	43,6	0	2553	0,437	0	0	1,19	0,043
Average	0,123	52,9	0,572	762	1,11	0,097	0,065	0,630	0,012
StDev	0,253	33,8	1,82	1256	1,40	0,270	0,161	1,03	0,018
Maximum	0,802	159	6,33	3753	4,22	0,949	0,562	3,30	0,044
Minimum	0	35,6	0	2,38	0	0	0	0	0
Chalcopyrite									
<u>Chalcopyrite</u>	<u>As75</u>	<u>Se77</u>	<u>Mo95</u>	<u>Ag107</u>	<u>Sb121</u>	<u>Te125</u>	<u>W182</u>	<u>Au197</u>	<u>Bi209</u>
WE-6A-5-A-CH	0	79,8	0,382	1069	1,86	0	0,018	0,026	0
WE-6A-14-C-CH	0	77,5	0,306	421	0,666	0,142	0	0	0
WE-6A-17-L-CH	5,64	78,8	0	692	5,47	0,664	0	0,012	0
WE-6A-19-K-CH	0,409	79,4	0,523	1052	1,59	0,446	0	0,273	0,007
WE-6A-24-M-CH	0	73,1	0	362	2,29	0,913	0,129	0,069	0
WE-6A-28-N-CH	0,122	84,7	0,664	945	0,704	0,226	0,034	0,060	0,007
WE-6A-31-N-CH	0	77,4	0	1070	0,174	0	0	0,035	0
WE-6A-33-N-CH	0,208	79,3	0,140	903	3,95	0,331	0	0,458	0,054
WE-6A-34-N-CH	0,012	91,6	0,045	876	0,938	0,347	0,087	0,123	0,377
WE-6A-39-H-CH	0,155	84,8	0	556	0,852	0	0	0,122	0,021
WE-6A-40-H-CH	0	83,8	0	483	0,809	0	0	0,067	0
WE-6A-44-H-CH	0,669	79,1	0,071	901	1,01	0	0	0,078	0
WE-6A-45-H-CH	0	83,7	0,629	833	0,346	0	0	0,053	0
Average	0,555	81,0	0,212	782	1,59	0,236	0,021	0,106	0,036
StDev	1,54	4,65	0,257	252	1,54	0,296	0,041	0,127	0,104
Maximum	5,64	91,6	0,664	1070	5,47	0,913	0,129	0,458	0,377

Minimum	0	73,1	0	362	0,174	0	0	0	0
<u>Sphalerite</u>	<u>As75</u>	<u>Se77</u>	<u>Mo95</u>	<u>Ag107</u>	<u>Sb121</u>	<u>Te125</u>	<u>W182</u>	<u>Au197</u>	<u>Bi209</u>
WE-6A-1-P-SP	0,034	8,06	0,143	4,44	0,133	0	0	0,128	0,055
WE-6A-6-A-SP	0,016	9,28	0,041	2,09	0	0,282	0	0	0
WE-6A-10-O-SP	0	9,79	0,162	8,07	0,179	0	0	0,034	0,018
WE-6A-16-L-SP	0	8,54	0,013	3,94	0,046	0	0	0,007	0
WE-6A-22-G-SP	0,025	7,94	0,118	1,31	0,072	0	0	0	0,009
WE-6A-25-M-SP	0	8,53	0,145	1,99	0,032	0,290	0	0,016	0
WE-6A-27-F-SP	0	7,57	0,009	1,63	0,101	0	0	0,030	0,008
WE-6A-37-H-SP	0,001	9,41	0,076	2,74	0,040	0	0	0	0
WE-6A-38-H-SP	0	10,2	0,086	3,97	0,089	0	0	0,048	0,047
WE-6A-48-H-SP	0	9,65	0,002	10,6	0,633	0,666	0	0,017	0
WE-6A-49-H-SP	0,031	10,8	0,006	9,48	0,416	0,118	0	0	0
Average	0,010	9,07	0,073	4,56	0,158	0,123	0	0,026	0,012
StDev	0,014	1,01	0,062	3,29	0,194	0,213	0	0,038	0,020
Maximum	0,034	10,8	0,162	10,6	0,633	0,666	0	0,128	0,055
Minimum	0	7,57	0,002	1,31	0	0	0	0	0
<u>Pyrite</u>	<u>As75</u>	<u>Se77</u>	<u>Mo95</u>	<u>Ag107</u>	<u>Sb121</u>	<u>Te125</u>	<u>W182</u>	<u>Au197</u>	<u>Bi209</u>
WE-7A-50-D-PY	105	5,33	0	0,070	1,36	0,029	0	0,003	0,007
WE-7A-52-D-PY	98,9	6,07	0	0,016	0	0	0	0	0,006
WE-7A-56-D-PY	163	5,33	0,021	0	0,134	0,153	0	0	0
WE-7A-57-D-PY	2,38	99,8	4,31	38,5	1,11	0	0	0	0
WE-7A-61-B-PY	87,3	10,8	0,085	1080	2,84	691	0	3,34	4,69
WE-7A-65-B-PY	90,9	4,71	0	7,31	3,95	8,13	0	0,113	2,23
WE-7A-68-K-PY	83,5	7,48	0	0,005	0,005	0,042	0	0	0
WE-7A-70-K-PY	64,1	11,2	0,125	0,001	0	0	0	0,003	0
WE-7A-75-M-PY	94,7	6,23	0	0,001	0,022	0,013	0	0,003	0
WE-7A-79-L-PY	82,4	6,08	0	0,012	0	0	0	0,006	0,010
WE-7A-80-L-PY	101	6,63	0,025	0,025	0	0,127	0	0	0
Average	88,4	15,4	0,415	102	0,857	63,6	0	0,316	0,631
StDev	37,6	28,1	1,29	324	1,37	208	0	1,00	1,50
Maximum	163	99,8	4,31	1080	3,95	691	0	3,34	4,69
Minimum	2,38	4,71	0	0	0	0	0	0	0
<u>Chalcopyrite</u>	<u>As75</u>	<u>Se77</u>	<u>Mo95</u>	<u>Ag107</u>	<u>Sb121</u>	<u>Te125</u>	<u>W182</u>	<u>Au197</u>	<u>Bi209</u>
WE-7A-51-D-CH	0	37,8	0	19,6	33,1	22,6	0	0,461	3,01
WE-7A-62-B-CH	66,9	10,9	0,044	4,51	3,69	3,00	0	0,312	5,12
WE-7A-63-B-CH	0	36,7	0,198	1,73	14,3	3,10	0	0,125	1,78
WE-7A-64-B-CH	0,414	38,7	0,283	0,500	3,38	1,84	0	0,118	0,280
WE-7A-69-K-CH	13,4	29,0	0	9,32	13,3	15,1	0	0,455	5,23
WE-7A-71-M-CH	21,0	32,8	0	17,2	38,2	11,1	0,013	0,316	9,22
WE-7A-72-M-CH	0,276	41,5	0,131	0,674	2,66	3,17	0	0,036	0,232
WE-7A-73-M-CH	0,279	40,5	0,066	0,348	1,46	0,901	0,017	0,036	0,111
WE-7A-74-M-CH	0	39,3	0	0,504	5,52	0,771	0	0,044	0,372
WE-7A-81-L-CH	0	28,0	0	1,47	41,9	2,06	8,93	0,206	1,14
Average	10,2	33,5	0,072	5,59	15,7	6,36	0,896	0,211	2,65
StDev	21,2	9,23	0,100	7,32	15,9	7,40	2,82	0,166	3,02
Maximum	66,9	41,5	0,283	19,6	41,9	22,6	8,93	0,461	9,22
Minimum	0	10,9	0	0,348	1,465	0,771	0	0,036	0,111
<u>Sphalerite</u>	<u>As75</u>	<u>Se77</u>	<u>Mo95</u>	<u>Ag107</u>	<u>Sb121</u>	<u>Te125</u>	<u>W182</u>	<u>Au197</u>	<u>Bi209</u>
WE-7A-53-D-SP	0,088	4,38	0,043	1,09	0,796	0,155	0	0,008	0,044
WE-7A-55-D-SP	0	2,96	0,156	57,37	5,52	139	0	4,449	0,207

WE-7A-66-B-SP	0,090	4,86	0,083	0,909	0,606	0	0	0,009	0,081
WE-7A-67-K-SP	0	3,89	0,005	6,80	9,50	16,63	0	0,206	0,565
WE-7A-76-M-SP	0	4,63	0	1,13	1,10	0,168	0	0,027	0,111
WE-7A-77-M-SP	0	2,25	0,117	0,949	2,56	0,790	0	0,024	0,146
WE-7A-84-L-SP	0	3,17	0,033	0,683	0,065	0	0	0	0
WE-7A-90-L-SP	0	2,30	0,032	0,637	0	0	0	0,018	0
Average	0,022	3,55	0,059	8,70	2,52	19,61	0	0,593	0,144
StDev	0,041	1,03	0,055	19,77	3,35	48,64	0	1,56	0,184
Maximum	0,090	4,86	0,156	57,37	9,50	139	0	4,449	0,565
Minimum	0	2,25	0	0,637	0	0	0	0	0
Galena	<u>As75</u>	<u>Se77</u>	<u>Mo95</u>	<u>Ag107</u>	<u>Sb121</u>	<u>Te125</u>	<u>W182</u>	<u>Au197</u>	<u>Bi209</u>
WE-7A-54-D-GA	0,085	794	0,011	740	268	710	0	0,112	1556
WE-7A-82-L-GA	0,087	1100	0	842	345	639	0,040	0,137	1516
WE-7A-83-L-GA	0	1196	0	758	315	693	0	0,127	1528
WE-7A-86-L-GA	0,067	1297	0,012	860	318	714	0	0,134	1588
WE-7A-87-L-GA	0	1292	0,008	790	214	663	0	0,165	1597
WE-7A-88-L-GA	0,135	1312	9,96	782	260	632	0,394	0,174	1566
WE-7A-89-L-GA	0,119	1265	0	719	258	606	0	0,281	1506
Average	0,070	1179	1,43	784	283	665	0,062	0,161	1551
StDev	0,053	185	3,76	51,8	45,1	41,7	0,147	0,057	35,3
Maximum	0,135	1312	9,96	860	345	714	0,394	0,281	1597
Minimum	0	794	0	719	214	606	0	0,112	1506

5. Discussion

5.1 Comparison of samples

All eight samples are affected by deformation and metamorphism and there are compositional and textural differences between them. The appearances of the samples differ in amount of sulphides present. The least altered dacites (sample WE-1 and WE-8) contains the lowest amount of sulphide minerals compared to the other samples, but both have pyrite as the most abundant mineral within them. The matrixes are similar, with a high abundance of quartz and sericite, with both displaying foliation. WE-3 and WE-4 both present larger abundance of sulphide minerals than those previous mentioned. They display strong foliation and several veins of aggregated quartz and calcite around the opaque minerals. None of these two samples display pyrrhotite, but they have aggregated and recrystallized pyrites with inclusions.

Sample WE-5 is a massive sulphide and contain minor silicate minerals evenly distributed through the sample. The pyrites contain the largest caries texture of all samples, and the grains are uneven around the edges. The two samples (WE-5 and WE-6) are from an Au-rich area where they are both characterised by mostly pyrite and sphalerite. There is higher abundance of pyrrhotite and chalcopyrite within WE-6 than in WE-5. The Au-poor sample WE-7 contain mostly pyrite and only minor grains of sphalerite, galena and chalcopyrite. The difference from the Au-rich and the Au-poor are the pyrrhotites in the Au-rich sample that is missing from the Au-poor. There is higher abundance of galena and it also forms as larger patches between the other surrounding sulphides in sample WE-7 compared to the others.

Pyrite occurs in all samples and displays both the texture of aggregate with many inclusions as well as single euhedral grains with relatively few or no inclusions. It is replaced by sphalerite, chalcopyrite and pyrrhotite and galena occurs as inclusions or between grains. This indicates that it is the first formed sulphide mineral in this region.

5.2 Interpretation of SEM and LA-ICP-MS data

The data supplied from the SEM and the LA-ICP-MS have both contributed to deeper knowledge about the mineralogy and Au content within Westwood deposit. Focus with the SEM was to identify sulphide minerals as a preparation for the LA-ICP-MS and both sulphide minerals and some nearby adjacent silicate minerals were analysed. The results display the ratio of the compositions within each mineral in all analysed samples. Au and Ag were detected with SEM and are only present in WE-5 and WE-6. This was presumed since they both represent Au-rich location. According to the SEM images and spectrum, Au occurs as electrum together with Ag as small grains between sulphide minerals.

The diagrams below display average of the elements in WE-6A and WE-7A for each of the spots analysed with LA-ICP-MS. In **Figure 21**, there is a similar trend for all the

sulphide minerals in sample WE-6A. They show lower contents of As, Mo and W and peaking in Se, Ag and Au. The largest amount is Ag in all minerals. Arsenic is the only element that clearly separates between the samples, being a higher value of 200 ppm in pyrite compared to chalcopyrite, pyrrhotite and sphalerite that all are below 0.5 ppm. The high amount of Ag together with chalcopyrite could indicate higher gold grade within an ore zone (Dubé and Mercier-Langevin et al., 2007).

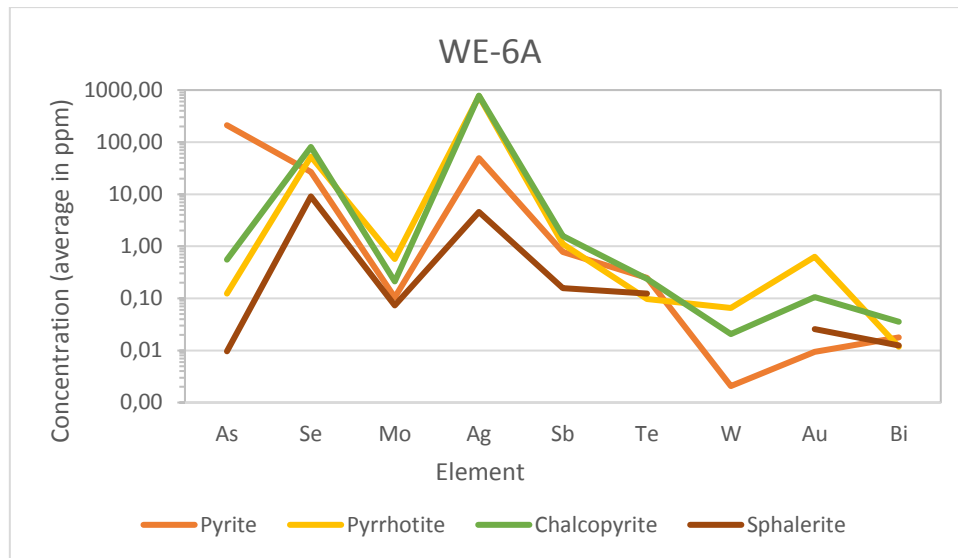


Figure 21. Diagram of average analysed trace elements in ppm for Au-rich sample WE-6A.

In sample WE-7A, there is larger spreading of the trace elements within the sulphide minerals (**Figure 22**). They all have lower concentration of Mo and W. As is found mainly in chalcopyrite, and like for WE-6A it is also hosted in pyrite. Galena has the highest content of each of the trace element except for W and Au. Ag is abundant in all the minerals but most enriched in galena with an average of 784 ppm.

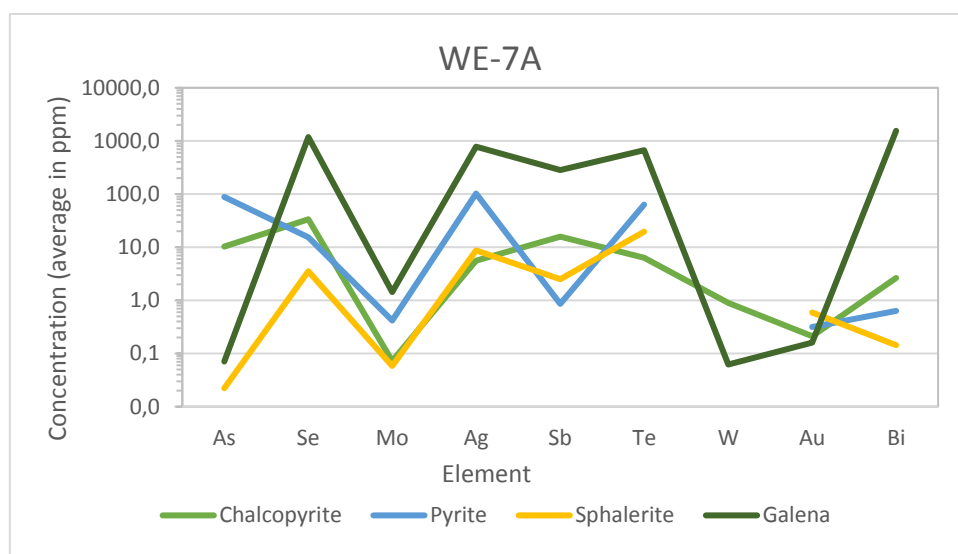


Figure 22. Diagram of average analysed trace elements in ppm for Au-poor sample WE-7A.

The element concentrations are in total higher within the sulphide minerals in the Au-poor sample than within the Au-rich. This could imply that the elements have been remobilized from the Au-rich sample and why the concentrations are lower within these sulphides, and that the majority of Au is found in separate grains of electrum. WE-6A and WE-7A contain pyrites with similar amount of trace elements in both samples but with less Au in WE-6A with an average of 0.009 ppm and for WE-7A it is 0.316 ppm.

5.3 Au enrichment in samples

The analyses from LA-ICP-MS displays that the amount of gold within the sulphide minerals in WE-6A are of lower values than for WE-7A. The gold between the sulphide minerals has formed during leaching of metal-rich hydrothermal fluids that has probably carried Au during magmatic events (Yergeau et al., 2015). The difference in mineralogical composition is the presence of pyrrhotite in the Au-rich samples and larger amount of galena seen in the Au-poor sample. These results can explain where the Au is located and it is noticeable that the main amount of Au is found as electrum together with Ag in sample WE-6A and that in WE-7A the Au appears as inclusions within sulphide grains.

According to the results from the LA-ICP-MS, Au is evenly distributed within all the sulphide minerals in the samples. The Au was probably first originated in the sulphides but was remobilised out during retrograde metamorphism.

Majority of the Au abundance in WE-6A sits within the pyrrhotite grains with the highest amount of 3.4 ppm. The second largest abundance is in chalcopyrite while sphalerite and pyrites show lower values. In WE-7A there is one peak value of Au content in each of pyrite (3.2 ppm) and sphalerite (4.3 ppm). All the other values are below 0.5 ppm. The Au-poor sample has the least amount of silicates and is a massive sulphide. Au is found present in a small quantity in each of the minerals in both samples. Evidence of electrum in sample WE-6A confirms the presence of gold that was already seen with the SEM.

In the diagram in **Figure 23**, the Au content is displayed for the Au-rich sample. Highest amount of Au is found within pyrrhotite, while least is within pyrite.

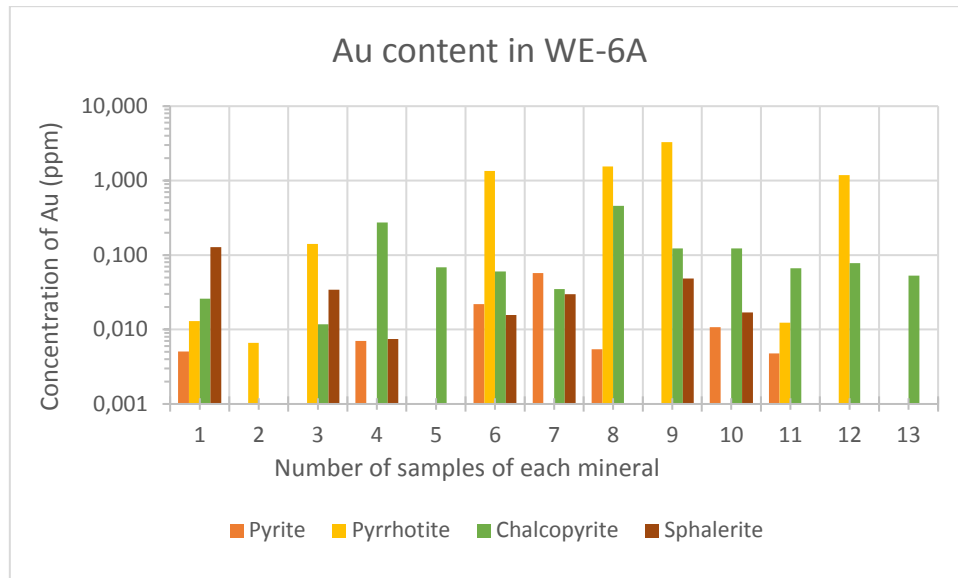


Figure 23. Au content in ppm in sample WE-6A

Sample WE-7A contains high amount of Au, for being from an Au-poor zone (**Figure 24**). Two peaks of gold are seen within sphalerite and pyrite. Except for those, the sample consist of a relatively equal abundance of Au. Compared to the Au-rich sample they display similar abundance even though the gold is more favoured in some minerals within WE-6A and some in WE-7A.

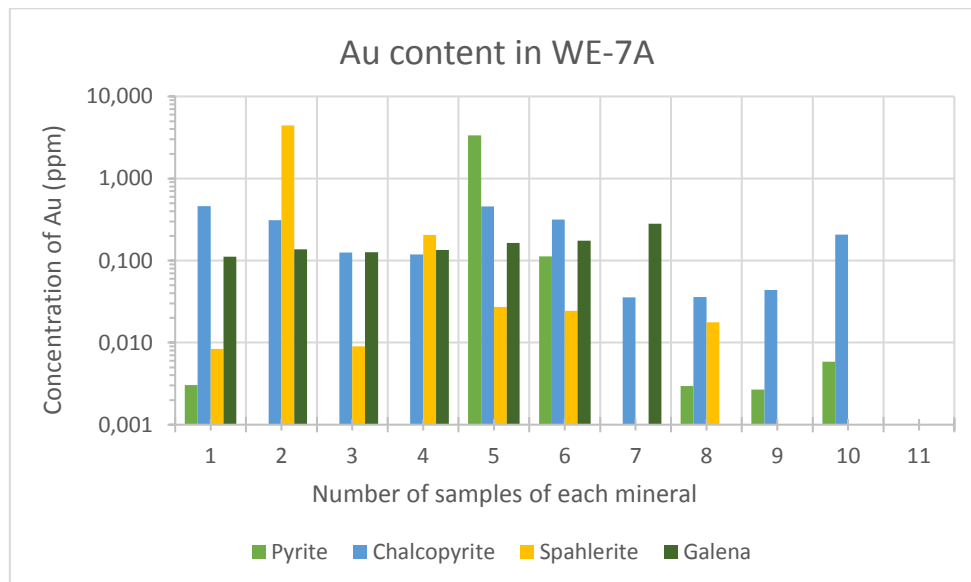


Figure 24. Au content in ppm in sample WE-7A.

5.4 Comparing Westwood deposit to Boliden Au-deposit

The occurrence of precious metals in VMS deposit is also well known in the Skellefte district in Sweden. The Boliden deposit, from which the exploration and mining company got its name, is one of the world's most Au rich VMS deposits with an average grade of 15 g/t. The Skellefte district where the deposit resides is Paleoproterozoic and the host rock is submarine volcanic rock and rhyolitic metavolcanics with hydrothermal alteration. The deposit displays some similarities to Westwood in that they were both subjected to deformation and metamorphosed to upper greenschist and lower amphibolite facies. The sulphide assemblage mostly consists of elongated lenses of pyrite and arsenopyrite, with minor traces of pyrrhotite and chalcopyrite. Free gold is present within veins and fractures between pyrrhotite and chalcopyrite. LA-ICP-MS has also been used for samples from Boliden for investigating the host minerals for Au enrichment (Wagner et al., 2007).

The results show that Au is found within pyrite and particularly arsenopyrite with convincing evidence for remobilisation of gold during metamorphic recrystallization of the deposits (Wagner et al., 2007). The largest amount of gold occurs within massive arsenopyrite (range of 3.8-108 ppm) and with lower concentration in recrystallized arsenopyrite (0.05-71.5 ppm) (Wagner et al., 2007). Massive pyrite and pyrite within gold-bearing veins also showed low abundance of gold (0-0.22 ppm and 0-0.19 ppm respectively). This data, together with textural observations, were interpreted as showing that a later metamorphic event had caused remobilisation of Au in Boliden deposit. The Au was leached to zones with lower strain within veins and fractures where it occurs as native gold (Wagner et al., 2007).

Similar processes are suggested to have occurred at Westwood. Even though the mineral assemblage at Westwood is different from Boliden and with no arsenopyrite, the process of Au remobilisation can be clearly observed. Both studies show that Au exists within sulphide minerals, but that the concentrations are low most likely due to remobilisation of the gold out of the sulphides into fractures where it occurs as native gold or electrum. But for the Au-poor sample it could be that the rock has not been enough recrystallized to the extent needed for Au to be released from the sulphide grains (Wagner et al., 2007).

5.5 Significance of study

Based on the data from LA-ICP-MS it is concluded that Au is found as a minor element within sulphide minerals in sample WE-6A and WE-7A from Westwood deposit. It is important to take into consideration that these samples only represent a small part of the area, and for extended work and research more samples must be collected and analysed to achieve a larger image of the Au-content in Westwood deposit. This is useful information for the processing of extracting Au from the host rock because then more elaborated techniques could be used for the Au inclusions. The fluctuation of prices for

precious and base metals make VMS deposits, like Westwood, a safer mining-process for mining companies to withstand low economic activities. It is important to investigate both the primary structures of the ore deposit as well as the formations that have undergone deformation and metamorphism, knowing that there is gold in the form of electrum present between sulphide minerals and that Au also form as inclusions.

6. Conclusion

The Abitibi belt is the host of several VMS deposits containing ore lenses, with the Westwood area among them. The aim of the project was to identify the sulphide mineralogy of samples from Westwood deposit and to investigate if and where it is possible to discover traces of Au or Au-alloys within eight samples of varied lithologies. Based on the results and discussion, it is clear that Au exist within both Au-rich ore zone and Au-poor zone. Size of the Au particles are smaller and exist as inclusions within sphalerite, pyrrhotite, galena, chalcopyrite and to lesser extent in pyrite in WE-7A, and as grains of electrum in WE-6A.

The distribution of Au within Westwood deposit could be extracted to a larger amount than it is today with the techniques to process the Au from the sulphide minerals and not only the free Au-Ag alloys that have been leached from recrystallized pyrites. One main aim was to locate the majority of the Au and results show that it is within electrum. Au occurred probably within the sulphides but was remobilised out during metamorphism. Au formed together with Ag the alloy electrum that is found in the Au-rich samples between the sulphide minerals, and it also explains the lower concentrations of Au within its sulphide grains. Since the results imply a sulphide reaction similar to that of the Boliden mine, it could conclude that there is a larger amount of Au in the Westwood deposit that could be extracted from Au inclusions within sulphide minerals as well as free grains of electrum.

7. Acknowledgements

First and foremost, I would like to thank my supervisor Iain Pitcairn for his great support and guidance during this project. Dan Zetterberg for his knowledge and help with rock cutting. Johan Högmalm, Axel Sjöqvist and Mikael Tillberg at Gothenburg University for helping with analysis with the LA-ICP-MS and Johan for all his work with the data reduction. Nicholas Leventis for helping with instruments and for bouncing ideas and information from the laser ablation analyses. Pernilla Berthelard and Dave Gallacher are thanked for their proof reading of this paper. I would like to thank the staff at the Department of Geological Sciences during my time of studying, and also thank my family and friends for their constant support.

8. References

- Dubé, B., Gosselin, P., Mercier-Langevin, P., Hannington, M., and Galley, A., 2007, Gold-rich volcanogenic massive sulphide deposits, in Goodfellow, W.D., ed., *Mineral Deposits of Canada: A Synthesis of Major Deposit-Types, District Metallogeny, the Evolution of Geological Provinces, and Exploration Methods*: Geological Association of Canada, Mineral Deposits Division, Special Publication No. 5, p. 75-94.
- Dubé, B., Mercier-Langevin, P., Hannington, M., Lafrance, B., Gosselin, G., Gosselin, P., 2007. The LaRonde Penna World-Class Au-Rich Volcanogenic Massive Sulfide Deposit, Abitibi, Québec: Mineralogy and Geochemistry of Alteration and Implications for Genesis and Exploration, *Society of Economic Geologists, Inc. Economic Geology*, v. 102, pp. 633–666.
- Galley, A., Hannington, M., and Jonasson, I., 2007. Volcanogenic massive sulphide deposits: Geological Association of Canada, Mineral Deposits Division, Special Publication 5, p. 141–161.
- Gibson, H. L., Allen, R. L., Riverin, G., Lane, T. E., 2007. The VMS Model: Advances and Application to Exploration, *Proceedings of Exploration 07: Fifth Decennial International Conference on Mineral Exploration*, p. 713-730.
- Günther, D., Hattendorf, B., 2005. Solid sample analysis using laser ablation inductively coupled plasma mass spectrometry, *Trends in Analytical Chemistry*, Vol. 24, No. 3, p. 255-265.
- Jochum K. P., Weis U, Stoll B, Kuzmin D, Yang Q, Raczek I, Jacob D, Stracke A, Birbaum K, Frick D. A., Gunther D, Enzweiler J., 2011. Determination of reference values for NIST SRM 610-617 glasses following ISO guidelines. *Geostandards and Geoanalytical Research*. 35:397–429.
- Mercier-Langevin, P., Wright-Holfeld, A., Dubé, B., Bernier, C., Houle, N., Savoie, A., and Simard, P., 2009. Stratigraphic setting of the Westwood-Warrenmac ore zones, Westwood Project, Doyon-Bousquet-LaRonde mining camp, Abitibi, Quebec; Geological Survey of Canada, *Current Research 2009-3*, 20 p.
- Onuk P, Melcher F, Mertz-Kraus R, Gäbler H. E., Goldmann S. 2016. Development of a matrix-matched sphalerite reference material (MUL-ZnS-1) for calibration of in situ trace element measurements by Laser Ablation- Inductively Coupled Plasma-Mass Spectrometry. *Geostandards and Geoanalytical Research*. doi:10.1111/.
- Sylvester P. J., Cabri L. J., Tubrett M. N., McMahon G, Laflamme J. H. G., Peregoedova A., 2005. Synthesis and evaluation of a fused pyrrhotite standard reference material for platinum group element and gold analysis by laser ablation-ICPMS. 10th International Platinum Symposium, Oulu, Geol Surv Finland, *Extend Abstr*, pp. 16–20.
- Vernon-Parry, K. D., 2000. Scanning Electron Microscopy: an introduction, *III-Vs Review*. Vol. 13, No 4, p. 40-44.

Wagner, T., Klemm, R., Wenzel, T. and Mattsson, B., 2007. Gold upgrading in metamorphosed analysis of invisible gold evidence from laser-ablation -inductively coupled plasma-mass spectrometry, *Geology* 2007;35; p. 775-778.

Wilson, S. A., Ridley, W. I., Koenig, A. E., 2002. Development of sulfide calibration standards for the laser ablation inductively- coupled plasma mass spectrometry technique. *J. Anal. At. Spectrom.* 17:406–409.

Yergeau, D., Mercier-Langevin, P., Dubé, B., Jackson, S., Malo, M., Bernier, C., and Simard, P., 2014. Synvolcanic Au-Ag±Cu-Zn-Pb massive sulphides, veins and disseminations of the Westwood deposit, Abitibi greenstone belt, Québec; Geological Survey of Canada, Open File 7482, 54 p. doi:10.4095/293117

Yergeau, D., Mercier-Langevin, P., Dubé, B., Malo, M., McNicoll, V. J., Jackson, S.E., Savoie, A., and La Rochelle, F., 2015. The Archean Westwood Au deposit, southern Abitibi: Telescoped Au-rich VMS and intrusion-related Au systems, *In: Targeted Geoscience Initiative 4: Contributions to the Understanding of Precambrian Lode Gold Deposits and Implications for Exploration*, (ed.) B. Dube and P. Mercier-Langevin; Geological Survey of Canada, Open File 7852, p. 177–191.

Figures

Title page: Left: Photo of Au-rich sample WE-6, Right: Photo of Au-poor sample WE-7: Evelina Rann

Figure 1-2: Yergeau, D., Mercier-Langevin, P., Dubé, B., Jackson, S., Malo, M., Bernier, C., and Simard, P., 2014. Synvolcanic Au-Ag±Cu-Zn-Pb massive sulphides, veins and disseminations of the Westwood deposit, Abitibi greenstone belt, Québec; Geological Survey of Canada, Open File 7482, 54 p. doi:10.4095/293117

Figure 3-24: Evelina Rann